Title

Photo-Controlled Release of NO and CO with Inorganic and Organometallic Complexes

Authors

Pierri, AE
Muizzi, DA
Ostrowski, AD
et al.

Publication Date

2015

DOI

10.1007/430-2014-164

Peer reviewed

Struct Bond (2015) 165: 1–46
DOI: 10.1007/430_2014_164

Published online: 30 October 2014

Photo-Controlled Release of NO and CO with Inorganic and Organometallic Complexes

Agustin E. Pierri, Dayana A. Muizzi, Alexis D. Ostrowski, and Peter C. Ford

Abstract The photochemical delivery of bioactive small molecules to physiological targets provides the opportunity to control the location, timing, and dosage of such delivery. We will discuss recent developments of the synthesis and studies of various metal complexes designed for targeted release of the bioregulatory diatomics nitric oxide and carbon monoxide. Of considerable interest are those systems where the NO or CO precursor and/or the photochemical product is luminescent such that imaging techniques allow one to identify the release location.

Keywords Carbon monoxide · Luminescence · Near-infrared excitation · Nitric oxide · PhotoCORM · PhotoNORM · Photoreaction

Contents

A.E. Pierri and P.C. Ford (✉)
Department of Chemistry and Biochemistry, University of California, Santa Barbara, Santa Barbara, CA 93106, USA
e-mail: ford@chem.ucsb.edu

D.A. Muizzi and A.D. Ostrowski (✉)
Department of Chemistry and Center for Photochemical Sciences, Bowling Green State University, Bowling Green, OH, USA
e-mail: alexiso@bgsu.edu

Abbreviations

4-vpy	4-Vinyl pyridine
AFX	2-Aminofluorene chromophores
BODIPY	Boron dipyrromethane difluoride
bpy	2,2′-Bipyridine
COP-1	Palladium dimeric complex
CORM	Carbon monoxide releasing moiety
COSer	Carbon monoxide sensitive biosensor
cpYFP	Circularly permuted yellow fluorescent protein
CrONO	*trans*-Cr^{III}(Cyclam)$(ONO)_2^+$
Cyclam	1,4,8,11 Tetraazacyclotetradecane
DFT	Density functional theory
DMF	Dimethylformamide
DMSO	Dimethylsulfoxide
dpa	*N*,*N*-bis(2-pyridylmethyl)amine
DPBS	Dulbecco's phosphate buffered saline
DPPQ	Diphenylphosphinoquinoline
EPR	Electron paramagnetic resonance
ES	Excited state
FLEt	Fluorescein ethyl ester
Fluor	Fluorescein
FRET	Förster resonance energy transfer
GSH	Glutathione
H_2bpb	1,2-bis(pyridine-2-carboxamido)benzene
H_2bqb	1,2-bis(quinoline-2-carboxamido)benzene
H_2IQ1	1,2-bis(isoquinoline-1-carboxamido)benzene
H-dpaq	2-[*N*,*N*-bis(pyridine-2-ylmethyl)]-amino-*N*′-quinoline-8-yl-acetamido
HO	Heme oxygenase
I	Incident light intensity
I_a	Intensity of light absorbed
iCORM	Inactive CORM
Im	Imidazole
IR	Infrared
LDH	Lactate dehydrogenase

LF	Ligand field
LLL	Tripodal polypyridine ligands
mac	5,7-Dimethyl-6-anthracyl-cyclam
Mb	Myoglobin
MLCT	Metal to ligand charge transfer
NIR	Near infrared
NMR	Nuclear magnetic resonance
NOA	Nitric oxide analyzer
OEP	Octaethylporphyrinato
$PaPy_2QH$	*N*,*N*-bis(2-pyridylmethyl)amine-*N*-ethyl-2-quinoline-2-carboxamide
$PaPy_3H$	*N*,*N*-bis(2-pyridylmethyl)amine-*N*-ethyl-2-pyridine-2-carboxamide
PEG	Polyethylene glycol
pHEMA	Poly(2-hydroxyethyl methacrylate)
photoCORM	Photo-activated CO releasing moiety
photoNORM	Photo-activated NO releasing moiety
PL	Photoluminescence
Por	Porphyrin
PPIX	Protoporphyrin-IX
pqa	(2-Pyridylmethyl)(2-quinolylmethyl)amine
py	Pyridine
QD	Quantum dot
RBS	Roussin's black salts
Resf	Resorufin
RRS	Roussin's red salts
RSE	Roussin's red esters
R-tpm	Tris(pyrazolyl)methane
Salen	*N*,*N*′-Ethylenebis(salicylideneiminato)dianion
Salophen	*N*,*N*′-1,2-Phenylenebis(salicylideneiminato)dianion
$SBPy_2Q$	*N*,*N*-bis(2-pyridylmethyl)amine-*N*-ethyl-2-quinoline-2-aldimine
$SBPy_3$	*N*,*N*-bis(2-pyridylmethyl)amine-*N*-ethyl-2-pyridine-2-aldimine
Seln	Selenophore
Sol	Solvent
TD-DFT	Time-dependent density functional theory
THF	Tetrahydrofuran
Thnl	Thionol
TMOS	Tetramethylorthosilicate
Tmp	Tris(hydroxymethyl)phosphine
tpa	Tris(2-pyridyl)amine
TPE	Two-photon excitation
TPP	Tetraphenylporphyrinato
TPPTS	Tris(sulfonatophenyl)phosphine trianion
UCNP	Upconverting nanoparticle
UV	Ultraviolet

1 Introduction: The Gasotransmitters Nitric Oxide and Carbon Monoxide

The discoveries several decades ago that nitric oxide (NO, aka nitrogen monoxide) is an endogenously produced bioregulator in mammalian (and human) physiology has stimulated a remarkable body of research into the biological activity of this diatomic free radical. It is now well established that NO plays important roles in vasodilation, neurotransmission, immune response, and apoptotic cell death [1]. Imbalances of NO, however, may also lead to various disease states such as cancer [2, 3] and cardiovascular diseases [4, 5]. Furthermore, NO can have contrasting physiological effects depending upon the localized concentration; if present in high amounts, it leads to tumor cell apoptosis [3], but low levels can lead to tumor proliferation [6]. Subsequent studies have shown that both carbon monoxide (CO) and hydrogen sulfide (H_2S) are also small molecule bioregulators [7–9].

Due to the multiple roles for nitric oxide in biological systems, there is considerable interest in the potential applications of compounds that release NO in a controlled and targeted manner (for examples, see [10–13]). One such strategy is the use of light as the trigger for NO release from appropriate precursors, given that this allows one to control the timing and location and potentially the dosage of such NO delivery in biological tissues. Consequently, a new generation of NO releasing compounds and materials have been developed, which involve transition metal complexes with metal nitrosyls, nitrates, and nitrites that are activated only by light [14–20]. The light-activated release of NO introduces targeting selectivity that systemic NO releasing drugs do not offer. Targeting might also be achieved by incorporating the photochemical NO precursor in a material for use as an implant, with the timing and dosage still controlled by photoactivation [13, 21–23]. For sake of simplifying our terminology, we will use the term “photoNORM” for such photo-activated NO releasing moieties.

Like NO, discussions of the biological activity of CO previously focused on toxicity, although it has been known for some time that CO is produced endogenously through heme oxidation by the enzyme heme oxygenase (HO) [24, 25]. Its endogenous production can be compared to that of nitric oxide [1], although its biologic activity has not been as thoroughly elucidated [26]. Like NO, CO has also been shown to be an important physiological signaling molecule [27], and exogenously applied CO has been implicated in various physiological effects, including preventing organ graft rejection, reducing ischemia-reperfusion injury, promoting wound healing, etc. [28–37]. Understandably, such biological effects have prompted a considerable interest towards developing targeted CO delivery techniques. To address this challenge, a class of carbon monoxide releasing moieties (CORMs) has been investigated [38–42]. These are typically metal carbonyls complexes that release a CO payload either by direct thermal decomposition, or triggered by environmental effects such as a change in pH, solvent, or temperature. Another approach that several laboratories are pursuing is to use light as the external trigger to stimulate CO release from photo-activated CO releasing moieties

(photoCORMs) [20, 42]. Again the advantage is that the use of light as an external trigger should provide excellent control of the location, timing, and dosage of CO release.

Key desirable features to be considered when designing photoNORMs or photoCORMs include the need to be sensitive to longer wavelength activation, since it is the red and near infrared (NIR) frequencies of light that have the deepest penetration through tissue [43]. A second would be reasonable stability under physiological temperatures and other conditions typical to living organisms, including stability toward an aerated, aqueous medium. A third would be the lack of undesirable toxicity either of the photochemical precursor or of the residual photoproduct after the bioactive small molecule is released. Achieving activation with red light is a challenge, however, since the energy required to break the bond between the metal center and NO or CO may be greater than the energy provided by the red light. Nevertheless, different strategies are being developed to generate the release of NO upon red light or NIR activation [44–53].

Another feature of interest in the design of photochemical precursors for such bioactive small molecules would be the ability to track their location and whether the system has indeed undergone the desired release at the target. Photoluminescence (PL) is a particularly sensitive imaging method in biological systems. Unfortunately, the majority of the molecular systems that display the desired properties as photoNORMs and photoCORMs tend to have at best, very weak PL properties; however, there are several well-defined exceptions. In the present review, we will describe the different classes of transition metal complexes that have been used for photochemical NO and CO release, the different methods that have resulted in the red light activation, those systems that demonstrate photoluminescence properties, and the development of new photoactive materials for use under biological conditions.

2 Nitric Oxide Releasing Compounds

Various transition metal complexes have been used as photoNORMs, and the photochemistry and reaction mechanisms of these are varied. Photoactive ruthenium, manganese, and iron-nitrosyl complexes are well known, and the mechanism of NO release involves the dissociation of the metal-NO bond. On the other hand, chromium and manganese can be coordinated to nitrite throughout the oxygen atom to form metal O-nitrito complexes, and these can generate nitric oxide by homolytic cleavage of the MO–NO bond. Figure 1 illustrates some examples of these metal nitrosyl and metal nitrite complexes.

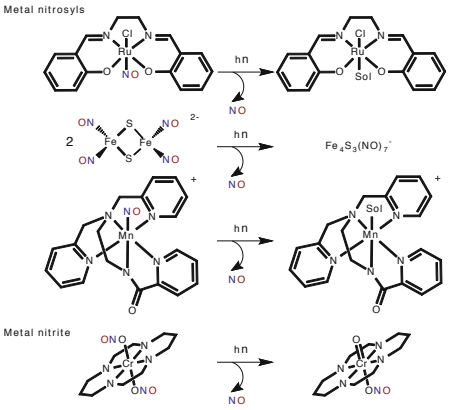

Fig. 1 Representative metal nitrosyl and metal nitrite complexes are shown along with the pathways for NO release after light irradiation

2.1 Metal Nitrito Complexes

2.1.1 Chromium Complexes

One extensively studied nitrito species is the *trans*-Cr^{III}(cyclam)$(ONO)_2^+$ (cyclam = 1,4,8,11 tetraazacyclotetradecane), also known as "CrONO." This chromium nitrito complex was designed considering that Cr is an oxophilic metal, and therefore, when nitrite is a ligand, the β-cleavage of the CrO–NO bond may be more favorable than the cleavage of the Cr–ONO bond [54, 55]. Changes in the absorbance spectrum when a deaerated solution of CrONO was subjected to long-term photolysis at 436 nm, did indicate the formation of the corresponding aquo complex (*trans*-Cr^{III}(cyclam)$(H_2O)(ONO)^{2+}$), the product of NO_2^- aquation; however, the quantum yield was relatively small (0.0092) [17, 18, 21]. In contrast, when CrONO was photolyzed in aerated solutions at irradiation wavelengths (λ_{irr}) between 365 and 546 nm, NO was generated at substantially higher quantum yields (Φ_{NO} up to 0.25). This difference can be interpreted in terms of the principal photoreaction being the reversible formation of the products NO and *trans*-Cr^{IV}(cyclam)(O)$(ONO)^+$ (Scheme 1). The back reaction occurs rapidly ($k_{NO} = 3.1 \times 10^{-6}$ M^{-1} s^{-1} at 298 K in aqueous solution) to regenerate the starting material (CrONO). Therefore, in order to maximize the net NO release, it is necessary to trap the Cr^{IV}

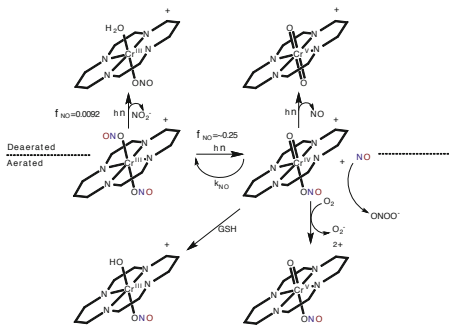

Scheme 1 Photochemical pathways of NO release from *trans*-Cr(cyclam)$(ONO)_2^+$ under both aerated and deaerated conditions and in the presence of the biological reductant glutathione (GSH) [18]

intermediate. This can be done with oxygen or with glutathione (GSH), an antioxidant agent present in biological tissue [18]. In this context, the photolysis was developed in the presence of GSH and analyzed both by absorbance changes and by direct measurement of NO by using a Sievers Nitric Oxide Analyzer (NOA). Both measurements gave a Φ_{NO} of 0.25 [17–19]. DFT computational studies as well as sensitizer and quenching studies suggest that the excited state (ES) responsible for homolytic cleavage of the CrO–NO bond is the doublet metal-centered (ligand field) state that is typically the lowest energy ES of such Cr^{III} complexes [18, 56].

In contrast with the results under aerated condition, photolysis of CrONO under a reduced oxygen atmosphere with the gaseous products being swept from the solution by entraining with helium, results in the generation of two moles of nitric oxide per mole of CrONO. Since no oxygen is present to trap the Cr^{IV} intermediate, this species apparently undergoes secondary photolysis to lose a second NO and to generate a Cr^{V} species, presumably the dioxo complex [18]. However, attempts to isolate and characterize this species quantitatively were unsuccessful.

The photolysis of CrONO in biological media has also been studied, in which it was shown that the NO release generates the vasorelaxation in porcine arteries by activating the enzyme soluble guanylyl cyclase [19]. Furthermore, CrONO and its photoproducts have been shown to be non-toxic toward THP-1 cells (a human monocyclic cell line) as evaluated with a lactate dehydrogenase (LDH) assay [18]. This lack of toxicity as well as the relative stability of CrONO at 37°C in aqueous media points to CrONO as a promising photoNORM. CrONO also displays relatively high quantum yield, but the low extinction coefficients and the

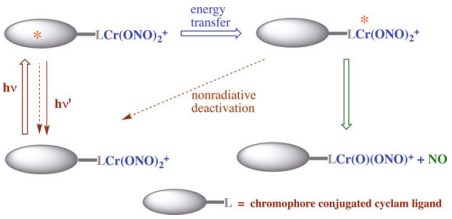

Scheme 2 Illustration of a CrONO derivative with an antenna chromophore such as anthracene or pyrene conjugated to the equatorial cyclam-type ligand. Excitation of the pendant antenna leads first to excitation of that chromophore, the excited state of which will decay by energy transfer to the Cr^{III} center or by nonradiative and radiative ($h\nu'$) deactivation to the original ground state (nonradiative deactivation shown as *dashed arrows*). Similarly, the metal-centered excited states of the Cr^{III} center can decay to the original ground state or undergo reaction to generate NO plus the Cr^{IV} oxo intermediate. The rate of NO release is the product of the intensity of the light absorbed (I_a) at λ_{irr} times the overall quantum yield (Φ_{NO}) for the photoreaction. Φ_{NO} is a function of the competitive rates of the various steps leading toward product formation vs. deactivation

wavelengths of the photoactive metal-centered absorption bands that lead to the NO production from CrONO are not ideal for therapeutic applications. Therefore, several strategies have utilized with the goal of triggering NO release from a CrONO derivative upon longer wavelength excitation. One of these is illustrated in Scheme 2.

In this context, DeRosa et al. [54] prepared Cr^{III} complexes of cyclam ligands modified by covalent attachment of antennas such as anthracene and pyrene. These compounds did not display the desired longer visible wavelength absorptions but did demonstrate that pendant chromophores can serve as antennae to gather light and to sensitize reactions localized at the Cr^{III} center. For example, the anthracene tethered complex *trans*-$[Cr(mac)(ONO)_2]BF_4$ (mac = 5,7-dimethyl-6-anthracyl-cyclam, Fig. 2) showed markedly enhanced rates of NO production when irradiated at 470 nm owing to the stronger absorption of the antenna at this λ_{irr}. Furthermore the anthracenyl fluorescence was largely attenuated, although a residual blue emission remained. Thus, energy transfer to the Cr^{III} center is efficient but not complete. Notably this residual emission proved to be especially valuable in tracking the presence of the *trans*-$Cr(mac)(ONO)_2^+$ ion when that salt was incorporated into liposomes, a potential carrier mechanism for delivery of this photoNORM to biological targets [57] (Fig. 2).

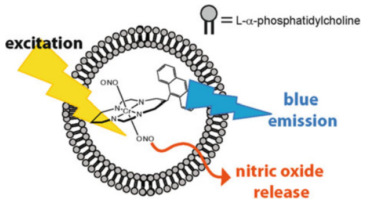

Fig. 2 Cartoon illustrating the encapsulation of the luminescent *trans*-Cr(mac)$(ONO)_2^+$ salts in liposomes [57] (the methyl groups of 5,7-dimethyl-6-anthracyl-cyclam are not shown). Reprinted with permission from Ostrowski et al. [57]. Copyright 2012 American Chemical Society

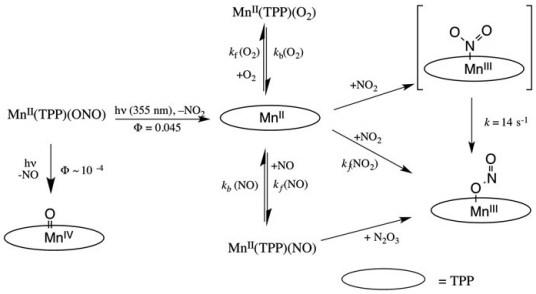

Fig. 3 Flash photolysis of Mn(TPP)(ONO) in presence of NO, NO_2, and O_2. Adapted from Halpenny et al. [22]

2.1.2 A Manganese Complex

In 1991, Watson and Suslick reported the NO photolability of Mn^{III}(TPP)(ONO) through the β-cleavage of the MnO–NO bond resulting in the formation of Mn^{IV}(TPP)(O) [58, 59]. However, the α-cleavage of Mn-ONO was also observed with the formation of Mn^{II}(TPP) and nitrogen dioxide. Subsequent laser flash photolysis studies (λ_{irr} 355 nm) by Hoshino et al. [60] showed the latter photoprocess to be the more efficient. The quantum yield of NO_2 release (Φ_{NO_2}) was 0.045 while Φ_{NO} was only ~10^{-4}. The complicated photochemistry of Mn(TPP)(ONO) results in the formation of several intermediates in presence of NO, NO_2, and O_2 [60] (Fig. 3). Nevertheless, manganese nitrito complexes show some

NO release after light irradiation and may be promising candidates for use in solid polymer platforms where the release of NO gas may be favored.

2.2 Metal Nitrosyls

Nitric oxide is a free radical in which the unpaired electron is in a π* orbital. When bound to a metal center, nitric oxide can either accept or donate electron density from or to the metal (Fig. 4). As a 3-electron donor, a linear M–NO bond angle of 180° is typical and the nitrosyl can be viewed as a nitrosonium cation (NO^+), with the corresponding NO stretching frequencies (ν_{NO}) between 1,820 and 2,000 cm^{-1}. This is typically observed with oxidizing metal centers such as Fe^{III}. With a more reducing center, NO can act as a 1-electron donor and the charge transfer is in the opposite direction to give a nitroxyl anion (NO^-) displaying a bent M–NO bond angle (~120°) with a much lower ν_{NO}. However, since the MNO unit is highly delocalized, it may be better to use the Enemark–Feltham notation $\{M–NO\}^n$, where n is the sum of the electrons in the NO π* orbital and the total number of *d*-electrons of the metal [61]. For example, the $\{Ru\text{-}NO\}^6$, notation used for many ruthenium nitrosyl complexes, has several resonance forms Ru^{II}-NO^+, Ru^{III}-NO, or Ru^{IV}-NO^-. While such species are indeed highly delocalized, Ru-NO complexes are most commonly viewed as Ru^{II}-NO^+ species based on EPR, IR, ^{1}H-NMR, and UV spectroscopic properties that indicate the bond order for NO to be greater than that of N=O [61–68].

2.2.1 Iron Complexes

A variety of iron-nitrosyl complexes (Fig. 5) have been demonstrated to be photochemically active toward NO photodissociation. Among these is sodium nitroprusside $Na_2[Fe(CN)_5NO]$, which has long been used therapeutically as a vasodilator during hypertensive emergencies [69]. Although photoactive [70, 71], nitroprusside can also release NO thermally upon contact with tissue containing

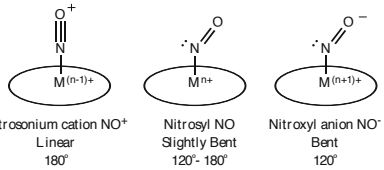

Fig. 4 Different structural forms of metal nitrosyl complexes

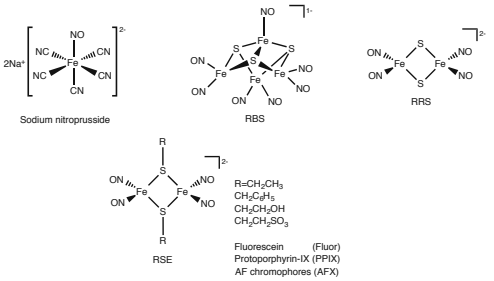

Fig. 5 Structures of the Fe-nitrosyl complexes that release NO photochemically

reducing species thereby limiting the photochemical control over the release of NO in this case.

The iron sulfur nitrosyl cluster anions Roussin's red salt (RRS) and Roussin's black salt (RBS) (Fig. 5) were first reported over 150 years ago by Roussin, and the latter was shown to affect the vascular tone of rat tail arteries, presumably by the slow release of NO [72, 73]. In 1997, Bourassa et al. demonstrated the quantitative photochemistry of both RRS and RBS and showed that NO released by visible wavelength irradiation of RRS was effective in sensitizing γ-radiation killing of hypoxic V-79 (Chinese hamster fibroblast) cells [73]. Since hypoxic regions of tumors are less susceptible to radiotherapy than normal tissue [74], this study demonstrated that simultaneous delivery of NO to a tumor site might enhance the effectiveness of such radiation treatment of cancer. For both RBS and RRS, NO release has been shown by laser photolysis studies to be reversible in deoxygenated solutions, especially in the presence of added NO [75]. However, in oxygenated solutions, photolysis led to more permanent changes, for example, Eq. (1).

$$Fe_4S_3(NO)_7^- \xrightarrow[O_2]{h\nu} 3{:}9Fe^{2+} + 5{:}9NO + 3S^{2-} + ? \quad (1)$$

Under such conditions, RRS is much more photoactive than RBS. For λ_{irr} between 313 and 546 nm NO generation from the RBS gave a modest Φ_{NO} of ~0.007 while Φ_{NO} values for RRS proved to be about an order of magnitude larger. NO release from RRS is dependent on the solvent, pH of the aqueous solution, and λ_{irr}. Photoreaction quantum yields for RRS varied from 0.004 (pH 7, deaerated aqueous solution, λ_{irr} 365 nm) to 0.4 (deoxygenated methanol, 365 nm), where aerated solutions showed a larger quantum yield (~0.1) than deoxygenated (0.004) and aerated organic solvents show even higher quantum yields. Computational studies using density functional theory (DFT) and time-dependent DFT (TD-DFT) of Fe/S/

NO clusters as well as for the ruthenium nitrosyls discussed below have attributed NO photolability to excited states (ES) displaying mixed $d(\text{metal}) \rightarrow p^*(\text{NO})$ charge transfer and $d \rightarrow d$ metal-centered character [71].

Ester derivatives of RRS have been used as photoNORMs, and these Roussin's red esters (RSE) are also illustrated in Fig. 5 [45, 76–78]. The RSE have analogous photochemistry to the RRS, where the largest quantum yields for NO release are seen in aerated solutions [77]. There was also a fast second-order back reaction of the RSE photoproduct with NO, so the net photochemistry is dependent on trapping of the Fe-photoproduct by oxygen [77].

The RSE have also been used to create red light activatable NO releasing compounds, where the ester derivative has a red light absorbing dye as antenna [45, 76, 78] in analogy to the systems described by Fig. 2. For example, PPIX-RSE [76] demonstrates enhanced rates of NO production upon red light photolysis owing to the much greater absorbances of the porphyrin Q bands at those wavelengths. Furthermore, although the fluorescence of the PPIX antenna is largely quenched by conjugation to the RSE iron/sulfur/nitrosyl cluster, there is some (~15–20%) residual emission, so that the presence of PPIX-RSE could be monitored with this feature. From measurements of the respective emission intensities for free PPIX and for PPIX-RSE and the characteristic lifetime of the former (~13 ns, [76, 79]) one can estimate rate constant for internal energy transfer from PPIX* to the cluster as $\sim 5 \times 10^8\ s^{-1}$. Ultrafast pulse laser emission lifetime measurements confirmed the partial quenching of PL from the PPIX antenna.

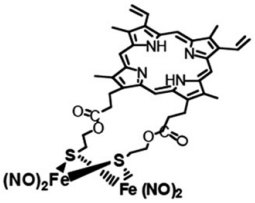

PPIX-RSE

As will be described below, PPIX-RSE can also be excited by 800 nm light from a pulsed ultrafast laser via two-photon absorption (TPA) at the PPIX antenna. This process was evidenced both by the weak emission at ~630 nm and by NO generation which was detected using a nitric oxide specific electrode [44]. Another approach to long wavelength NO photogeneration was to encapsulate RBS in NIR absorbing nano-carriers to give effective NO release after 980 nm excitation [51, 80]. These systems contain upconverting nanoparticles (UCNPs) that upon NIR excitation emit visible light that is reabsorbed by the photoNORM to release

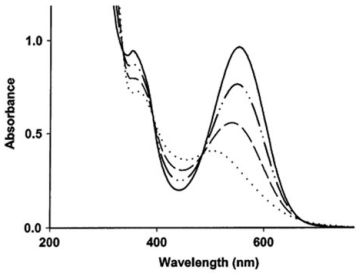

Fig. 6 Absorbance spectrum of $[Fe(PaPy_3)(NO)](ClO_4)_2$ in acetonitrile where absorbance changes are shown after light activation with a 50 W tungsten lamp (initial: *dotted line*; final: *solid line*) [81]. Reprinted with permission from Patra et al. [81]. Copyright 2003 American Chemical Society

NO, and as a result can be tracked via their upconverted emitted light. Both the two-photon excitation (TPE) and upconversion methods of utilizing NIR light for such purposes will be described more fully below.

In 2002, Patra, Mascharak, and co-workers reported the NO photo-releasing properties of iron-nitrosyl complexes with several carboxamide-containing pentadentate ligands [50, 81]. Inspired by the structure of the photoactive enzymenitrile hydratase, which contains an iron center coordinated to two carboxamides groups, they prepared the diamagnetic low spin $\{FeNO\}^6$ species $[Fe(PaPy_3)(NO)](ClO_4)_2$ ($PaPy_3H = N$,*N*-bis(2-pyridylmethyl)amine-*N*-ethyl-2-pyridine-2-carboxamide). This releases NO upon visible light activation with a Φ_{NO} of 0.185 at λ_{irr} 500 nm in acetonitrile (Eq. 2, Fig. 6). The ligand $PaPy_3^-$ contains a carboxamide group in with the σ-donating anionic nitrogen atom positioned *trans* to the NO to enhance the NO photolability. However, the stability of this complex in biological media is poor [81, 82]. From DFT calculations, it was observed that the electronic transition that labilizes NO occurs from a bonding Fe–NO orbital with a partial carboxamide character to an antibonding Fe–NO orbital.

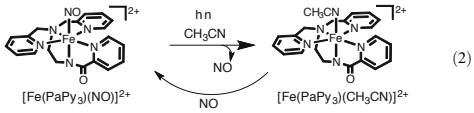

(2)

2.2.2 Manganese Complexes

Eroy-Reveles, Mascharak et al. [48] also prepared the analogous $[Mn(PaPy_3)(NO)]ClO_4$. This $\{Mn\text{-}NO\}^6$ complex irreversibly releases NO upon visible light activation (500–600 nm) affording the corresponding solvento Mn^{III} species (Eq. 3). The NO photolability was observed in acetonitrile, DMF, and water solutions, with NO

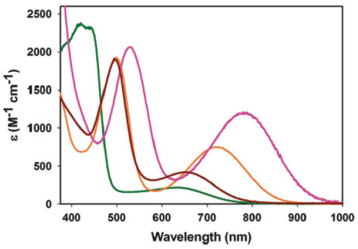

Fig. 7 Absorption spectra of $[Mn(SBPy_2Q)(NO)](ClO_4)_2$ (*pink*), $[Mn(SBPy_3)(NO)](ClO_4)_2$ (*orange*), $[Mn(PaPy_2Q)(NO)]ClO_4$ (*red*), and $[Mn(PaPy_3)(NO)]ClO_4$ (*green*) in acetonitrile [65]. Reprinted with permission from Hoffman-Luca et al. [65]. Copyright 2009 American Chemical Society

release increasing with the solvent (CH_3CN> DMF> H_2O) [83]. The Φ_{NO} values reported for this complex in acetonitrile are 0.33 and 0.31 at λ_{irr} 500 and 550 nm, respectively.

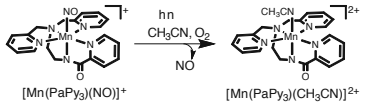

(3)

Greater sensitivity to red light was achieved by replacing one pyridine of $PaPy_3$− by a quinoline to give $PaPy_2QH$ (*N*,*N*-bis(2-pyridylmethyl)amine-*N*-ethyl-2-quinoline-2-carbox-amide). Spectral shifts due to the extended conjugation are evident in the absorption spectrum of $Mn(PaPy_2Q)(NO)^+$ (Fig. 7) [48]. Aqueous solutions of $Mn(PaPy_3)(NO)^+$ and $Mn(PaPy_2Q)(NO)^+$ gave Φ_{NO} values of 0.40 and 0.74 at 500 nm, 0.39 and 0.69 at 550 nm, respectively. The quantum yield decreases at longer wavelengths, but $Mn(PaPy_2Q)(NO)^+$ is still photoactive under NIR excitation at 810 nm. Computational studies by Merkle et al. [84] using TD-DFT [84] suggest that NO photolability is induced by population of excited states (ES) formed by transitions from Mn–NO bonding (d_π–π^*) orbitals into the Mn–NO antibonding (π^*–d_π) orbitals. These can be formed by direct excitation or by internal conversion/intersystem crossing from ES populated by excitation of more intense metal to ligand charge transfer (MLCT) absorptions.

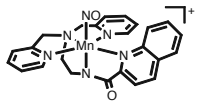

$[Mn(PaPy_2Q)(NO)]^+$

Other manganese-based photoNORMs described by this group utilized pentadentate ligands similar to $PaPy_3^-$ and $PaPy_2Q^-$ but with an imine nitrogen (rather than a carboxamide) *trans* to NO [65]. The manganese nitrosyls $[Mn(SBPy_3)(NO)](ClO_4)_2$ and $[Mn(SBPy_2Q)(NO)](ClO_4)_2$ absorb strongly at even longer wavelengths (Fig. 7) and have been shown to be photoactive toward NO release upon 800–950 nm light activation. However, the $Mn(SBPy_2Q)(NO)^{2+}$ cation is unstable in aqueous solutions [65].

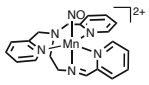

$Mn(SBPy_3)(NO)^{2+}$

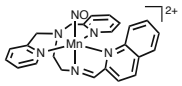

$Mn(SBPy_2Q)(NO)^{2+}$

Hitomi et al. [85] recently reported the photochemistry of related manganese nitrosyl complexes with the pentacoordinate anion of H-dpaq as the ligand framework (H-dpaq = 2-[*N*,*N*-bis(pyridine-2-ylmethyl)]-amino-*N*′-quinoline-8-yl-acetamido). This pentadentate ligand was modified by adding substituents (R = OMe, Cl, and NO_2) *para* to the carboxamide group, and the NO releasing properties of these derivatives were studied at $\lambda_{irr} = 350$, 460 and 650 nm. For more electron-donating groups (H and OMe), the highest quantum yields (0.58 and 0.61, respectively) were seen for excitation at 460 nm. However, for electron-withdrawing groups (Cl and NO_2), the λ_{irr} leading to the most efficient NO release was 650 nm with the respective Φ_{NO}'s 0.73 and 0.78. The various manganese nitrosyl complexes showing strong absorptions and photosensitivity at longer wavelengths (Fig. 7) would appear to be very promising photoNORMs [86].

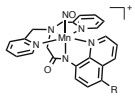

$[Mn((R)dpaq)(NO)]^+$

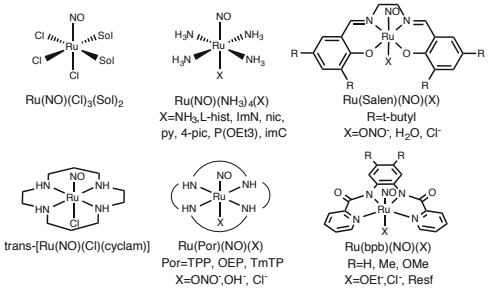

Fig. 8 Examples of NO photo-releasing ruthenium complexes

2.2.3 Ruthenium Complexes

Ruthenium nitrosyl complexes are generally quite robust, and this thermal stability as well as the known photolability of such species has drawn considerable attention to these as possible photoNORMs [20, 63, 67, 87–101]. Several representative complexes are illustrated in Fig. 8. We will discuss several examples.

One such ruthenium nitrosyl is the cyclam complex *trans*-[Ru(NO)(Cl)(cyclam)]$^{2+}$ prepared by Tfouni and co-workers. This {Ru-NO}^{6} species releases NO upon near-UV activation in aqueous solution with pH dependent quantum yields (Eq. 4). At pH 7.4 Φ_{NO} equals 0.16 [102].

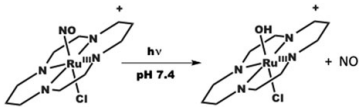

(4)

Early studies by Lorković and co-workers probed the photochemistry of various ruthenium(II) porphyrin nitrosyl complexes Ru(Por)(X)(NO) ($X^- = Cl^-$ or ONO, Por^{2-} = for examples, TPP^{2-}, tetraphenylporphyrinato, or OEP^{2-}, octaethylporphyrinato) [101, 103, 104]. Upon 355 nm flash excitation, these complexes reversibly released NO to give the Ru^{III}(Por)(X) intermediate, the second-order back reaction displaying rate constants $k_{NO} = 3–5 \times 10^8$ M^{-1} s^{-1}, in benzene. When X^- is ONO^-, photodissociation of NO_2^- also occurs to give the {Ru-NO}^{7} species Ru^{II}(Por)(NO), which, under excess NO, reacts rapidly to form a dinitrosyl complex Ru^{II}(Por)$(NO)_2$.

Another ruthenium nitrosyl platform encompasses the salen complexes Ru(salen)(X)(NO) (salen = *N*,*N*′-ethylenebis(salicylideneiminato)dianion, X = Cl^-,

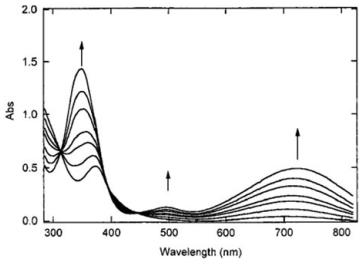

Fig. 9 Absorbance changes for 365 nm photolysis of Ru (Salen)(ONO)(NO) in acetonitrile

H_2O, ONO^-) and the analogous salophen complexes Ru(salophen)(X)(NO) (salophen = *N*,*N*′-1,2-phenylene-bis(salicylideneiminato)dianion) [21, 91, 99]. Works et al. showed that photolysis of these photoNORMs leads to NO labilization and formation of the corresponding solvento species Ru^{III}(salen)(X)(Sol), which display a characteristic UV band at 700–800 nm (Fig. 9). However, flash photolysis of these complexes under added NO shows a facile back reaction that is markedly sensitive to the nature of the solvent (and of the solvento complex, Eq. (5) [91, 99]. The rate constants k_{NO} for the back reaction in acetonitrile, THF, CH_2Cl_2, toluene, and cyclohexane, have values in the ranges 10^{-2}–10^{-4}, 10^{-2}, 10^{-1}, 10^6–10^7, and 10^6–10^8 M^{-1} s^{-1}, respectively [91, 99].

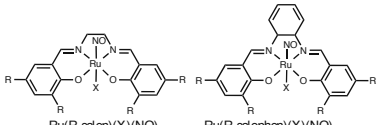

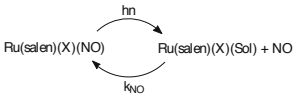

(5)

As a consequence, in donor solvents such as THF, water, acetonitrile, NO photolabilization from Ru(salen)(X)(NO) complexes is effectively irreversible.

For example, 365 nm photolysis of Ru(salen)(X)(NO) in acetonitrile gave a Φ_{NO} of 0.13. This falls off at longer λ_{irr}; 546 nm irradiation gives a Φ_{NO} of 0.07. Another factor is the nature of the axial ligand *trans* to NO; over the series $X = Cl^-$, ONO^-, H_2O, Φ_{NO} also decreases by more than an order of magnitude [63, 91, 99].

Rose et al. [105] have also prepared ruthenium nitrosyl complexes of the $PaPy_3^-$ anion described above. As noted for the analogous iron and manganese complexes, this places a σ-donating negatively charged nitrogen base positioned *trans* to the Ru–NO bond, thus stabilizing this moiety even in basic solutions. However, while $[Ru(PaPy_3)(NO)](BF_4)_2$ is more stable thermally than the iron analog, it required irradiation in the near-UV to labilize NO (Φ_{NO}, = 0.12 for λ_{irr} 355 nm under physiological conditions) [105, 106]. Extending the conjugation by using $PaPy_2Q^-$ as the chelating ligand (see above) gave greater lability at longer wavelengths. Photolysis of a $[Ru(PaPy_2Q)(NO)](BF_4)_2$ solution releases NO with a Φ_{NO} of 0.17 at λ_{irr} 410 nm.

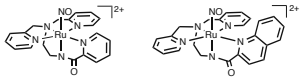

$[Ru(PaPy_3)(NO)]^{2+}$

$[Ru(PaPy_2Q)(NO)]^{2+}$

These workers also probed the influence of the carboxamide group on the photochemistry of similar $\{RuNO\}^6$ complexes by preparing ligands with different numbers of this functionality. Having more carboxamide groups resulted in a higher bathochromic effect, higher quantum yields, and a better stability under physiological conditions [90, 107, 108]. An example is the tetradentate anionic ligand bpb^- containing two carboxamide groups (H_2bpb = 1,2-bis(pyridine-2-carboxamido) benzene) from which they prepared the ruthenium complexes Ru(bpb)(NO)(X) ($X = Cl^-$, py, Im, OH^-, Resf) (Resf = resorufin). Different ligands X are in the position *trans* to NO since this coordination site is not occupied by the H_2bpb, and such ligands influence the reactivity, perhaps due to a *trans*-labilization effect [108]. Also altering the NO release efficiency are modifications of the H_2bpb ligand by adding substituents or increasing the conjugation. Increasing the electron-donating strength of the phenyl group (H < Me < OMe) resulted in a bathochromic effect of the *d*(Ru)-π(NO) → *d*(Ru)-π*(NO) transition and corresponding quantum yield increases [90, 107, 108].

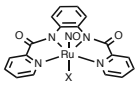

[Ru(bpb)(NO)(X)]
X= Cl-, OH-, Im, py

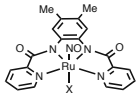

$[Ru(Me_2bpb)(NO)(X)]$

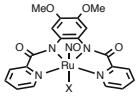

$[Ru((OMe)_2bpb)(NO)(X)]$

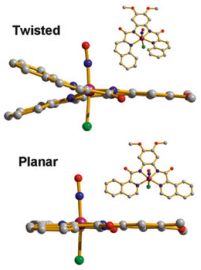

Fig. 10 X-ray structures of Ru((OMe)$_2$bQb)(NO)(Cl) (*top*) and Ru((OMe)$_2$IQ1)(NO)(Cl) (*bottom*) showing the steric interactions leading to non-planarity of the bQb ligand [90]. Adapted with permission from Fry and Mascharak [90]. Copyright 2011 American Chemical Society

Extending the conjugation of the carboxamide pyridyl group by using a quinoline (H_2bQb) or isoquinoline (H_2IQ1) gives complexes with a red-shifted *d*(Ru)-π(NO) → *d*(Ru)-π*(NO) transition and higher NO release efficiency. For example Φ_{NO} values of 0.010, 0.025, and 0.035, respectively were observed for 500 nm photolysis of DMF solutions of Ru((OMe)$_2$bpb)(NO)(Cl), Ru((OMe)$_2$bQb)(NO)(Cl), and Ru((OMe)$_2$IQ1)(NO)(Cl) [90, 107, 108]. Interestingly, the more sterically crowded Ru((OMe)$_2$bQb)(NO)(Cl) (Fig. 10) is less photoactive than the isoquinoline analog Ru((OMe)$_2$IQ1)(NO)(Cl) [32].

2.3 Polymers and Other Platforms

In this section, we will discuss the development of materials for the targeted release of NO in cells and tissues upon red light activation. For example, many of the complexes already mentioned above have been incorporated in platforms such as polymers and hydrogels. The ideal polymeric matrixes for such purposes should be biocompatible and optically transparent in order to deliver NO photochemically to the desired site. One method involves incorporation of a photoNORM into the polymer via covalent attachment, thereby preventing undesirable leakage into the host. For example, Borovik and co-workers have prepared a highly cross-linked methacrylate-based polymer matrix that incorporates a ruthenium salen nitrosyl complex that maintains its NO releasing properties (Fig. 11). This polymer is porous, with an average pore diameter of 60 Å and a λ_{max} of 373 nm in toluene [23]. The NO release analysis was carried out under different solvents, and the same solvent dependence characteristic of other ruthenium salen nitrosyls was observed [99]. The polymer releases NO under near-UV (370 nm) excitation, and NO release was detected by NO transfer to myoglobin (Mb) [23].

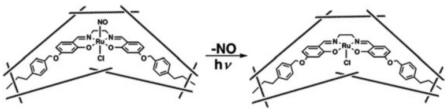

Fig. 11 Photoactive polymer matrix containing a ruthenium salen photoNORM [109]. Reprinted with permission from Welbes and Borovik [109]. Copyright 2005 American Chemical Society

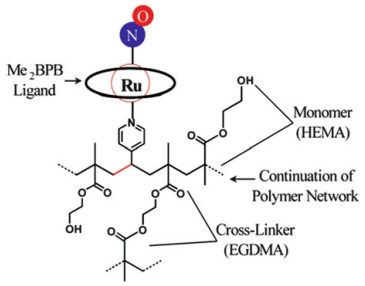

Fig. 12 Cross-linked pHEMA covalently attached to $Ru(Me_2bpb)(NO)(4\text{-}vpy)^+$ [22]. Reprinted with permission from Halpenny et al. [22]. Copyright 2007 American Chemical Society

Similarly, Halpenny et al. [22] covalently attached $Ru(Me_2bpb)(NO)(4\text{-}vpy)^+$ (4-vpy = 4-vinylpyridine) to the poly(2-hydroxyethyl methacrylate) (pHEMA) backbone cross-linked with ethyleneglycol dimethacrylate (Fig. 12). The resulting material released NO with a Φ_{NO} of 0.11 (determined amperometrically and by transfer to Mb) upon 350 nm excitation, a value only a little attenuated from that seen for the complex in solution (0.18).

Another approach to NO releasing materials is the encapsulation of known photoNORMs in polymeric gels [21, 22, 51, 86, 110–115]. For example, Bordini et al. [21] encapsulated the ruthenium nitrosyl $Ru(salen)(H_2O)(NO)^+$ in a silica sol-gel to give a material which released NO upon visible light excitation, and, more interestingly, could be regenerated by reaction of the photolyzed sol-gel with acidic nitrite and a reducing agent such as Eu^{2+} (Fig. 13).

In a similar context, Eroy-Reveles et al. [48, 86] have encapsulated $[Mn(PaPy_3)(NO)]ClO_4$ and $[Mn(PaPy_2Q)(NO)]ClO_4$ into a silicate sol-gel matrix with polyurethane or tetramethylorthosilicate (TMOS) (used to avoid the leakage of the complexes). Consistent with the much greater photolability of these manganese complexes at longer wavelengths (see above), the resulting materials release NO

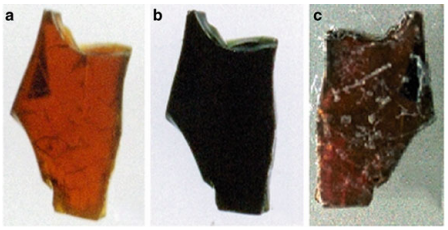

Fig. 13 $Ru(Salen)(H_2O)(NO)^+$ sol-gel images before (a) and after (b) photolysis and the regenerated starting sol-gel (c) [21] (Image supplied by Prof. E. Tfouni)

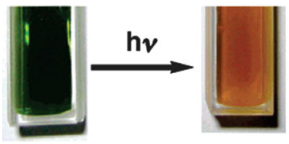

Fig. 14 Photolysis leads to color change of the sol-gel containing $[Mn(PaPy_3)(NO)]ClO_4$ [86]. Adapted with permission from Eroy-Reveles et al. [86]. Copyright 2006 American Chemical Society

upon visible and NIR light irradiation (Fig. 14). Although somewhat attenuated from the Φ_{NO} measured for $[Mn(PaPy_3)(NO)]ClO_4$ in aqueous solution (0.55), a substantial quantum yield of 0.25 was reported for 532 nm irradiation of the corresponding sol-gel formulation. This sol-gel matrix also rapidly delivers NO to Mb upon visible illumination by an optical fiber catheter incorporated into the polymer [112]. Moreover, the sol-gel encapsulated $[Mn(PaPy_2Q)(NO)]ClO_4$ is able to deliver NO to Mb upon 780 nm light irradiation [48].

2.4 Toward Longer Wavelength Activation

Many of the NO releasing complexes and materials previously discussed exhibit NO photolability, but do so only at the short wavelengths that have poor transmittance through skin and tissue. As a result, various strategies have been designed to make such species more susceptible to longer wavelength excitation [45, 48, 51, 52, 54, 76, 80, 85, 90, 116–119]. With certain platforms, it has proved possible to achieve the NO release at longer wavelength by extending the conjugation of the ligand frame and by

adding key substituent groups at strategic positions [65, 85, 90]. However, another approach is to develop antenna-photoNORM conjugates such as illustrated in Scheme 2, where the strongly absorbing antenna harvests one or more photons in order to form excited states from which energy transfer to the photoNORM occurs. The result is a sensitized photoreaction of the photoNORM that depends on the presence of excited states with appropriate energies and desired reactivities but does not depend on population of those states by direct absorption of light.

Such antennas can be directly attached to the ligand frame or coordinate to the metal center. Alternatively, in some cases the antenna and photoNORM can be held in close proximity by a viscous medium (such as a polymer) or by electrostatic effects. Examples of antennas covalently attached to ligand frames are the CrONO derivative *trans*-Cr(mac)$(ONO)_2^+$ [54] and the Roussin's red salt ester PPIX-RSE [76] described above. In both cases, the antennas retain a weak fluorescence and (in principle) their locations could be imaged via this property [57].

Examples of direct attachment of a dye antenna to the metal center are illustrates as Ru($(OMe)_2$IQ1)(NO)(dye), where in this case the dye is resorufin (Resf) if X = O, thionol (Thnl) if X = S, or selenophore (Seln) if X = Se. Fry et al. [107] have shown that 500 nm excitation of this chromophore in such complexes leads to significantly higher values of Φ_{NO} than for the analogous chloro complexes. Furthermore, the higher absorbances at these wavelengths should also increase the rate of NO production at comparable concentration. The absorption bands of these complexes shift to longer wavelengths as X is varied from O to S to Se (Fig. 15). As a result, Ru($(OMe)_2$bQb)(NO)(Seln) proved to be photoactive at $\lambda_{irr} = 600$ nm with a modest Φ_{NO} of 0.04 [47].

Another interesting feature is that Resf complexes retain residual fluorescence, although it is strongly quenched from that of free Resf in room temperature solution [120]. For example, Ru(Me_2bpb)(NO)(Resf) (Me_2bpb = 1,2-bis(pyridine-2-carboxamido)-4,5-dimethyl-benzene) in aqueous phosphate buffer (pH 7.4) exhibits a broad, low intensity fluorescence at ~580 nm that is sufficient to see in individual cells of human mammary cancer MDA-MB-231 cell cultures. Since NO dissociation leaves the Resf coordinated to a paramagnetic Ru(III) center, the fluorescence is quenched. Thus, this complex serves as a "turn-off" indicator of NO release. A similar system is Ru(Me_2bpb)(NO)(FlEt) (FlEt = fluorescein ethyl ester) [121]. Again, coordination of the strongly absorbing dye enhances the photolability of the coordinated NO at longer wavelengths (500 nm). In aqueous solution, the photoproduct of NO dissociation undergoes further aquation of the $FlEt^-$ moiety to "turn-on" fluorescence from the free FlEt unit.

Another approach to longer wavelength excitation is multiphoton excitation, which involves combining the energy of more than one NIR photon to achieve the energies necessary to effect the desired photochemistry from a suitable precursor [53]. A second potential advantage of this approach is that, since the probability of TPE is proportional to the square of the incident light intensity (I^2), it is most likely to occur at the focal point of the excitation beam. Thus, with a photoNORM sensitized by a two-photon absorbing dye, it should be possible to use this property to achieve greater spatial resolution in NO delivery using NIR excitation

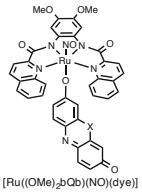

[Ru((OMe)$_2$bQb)(NO)(dye)]

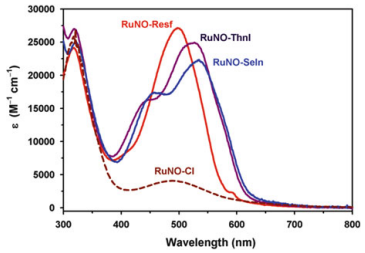

Fig. 15 Spectra of Ru((OMe)$_2$bQb)(NO)(dye), dye = Resf, Thnl or Seln). Reprinted with permission from [49]. Copyright 2009 American Chemical Society

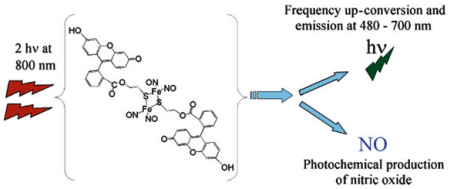

Fig. 16 Two-photon excitation of Fluor-RSE

wavelength appropriate for medical applications where tissue penetration is needed. The TPE of PPIX-RSE described briefly above [44] is the first example of such a technique applied to a photoNORM, but this has been followed by additional examples [45, 47, 51, 78].

One such example is Fluor-RSE, a Roussins red salt ester that has two fluorescein dye molecules attached to the iron sulfur cluster (Fig. 16). The resulting compound remains fluorescent but the steady-state PL is quenched about 85%

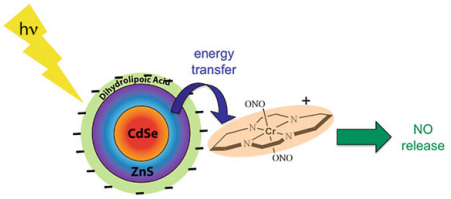

Fig. 17 Representation of NO release from *trans*-Cr(cyclam)$(ONO)_2^+$ using a CdSe/ZnS core/shell QD (surface modified with dihydrolipoate) as a photosensitizer. From [124]. Reprinted with permission from Burks et al. [124]. Copyright 2012 American Chemical Society

relative to the free dye in solution [46]. The quantum yield in aqueous solution for photodecomposition at 436 nm excitation was only 0.0036, although since all four NOs were released, $\Phi_{NO} = \sim 0.014$. More interestingly TPE of Fluor-RSE with intense pulses of light at a NIR wavelength (800 nm) leads both to NO generation and to fluorescence from the fluorescein chromophore. Subsequent studies have shown that the TPE technique with photoNORM conjugates can be used to deliver NO to cells [78] and to tissue [51].

Another strategy that has been applied is to use semiconductor quantum dots (QDs) and related nanoparticles as the light-gathering antenna to sensitize photoNORMs [51, 80, 119, 122]. Quantum dots have very large extinction coefficients for single photon absorption as well as very high two-photon absorption cross sections. Another very important feature is that the photophysical behaviors of semiconductor QDs are strongly dependent on the nanoparticle shape and size, the band edge absorption and emission bands shifting to longer wavelength with increasing diameter. Furthermore, the QD surfaces can, in principle, be decorated not only with a photochemical precursor of a bioactive small molecule but also with targeting moieties to make these multifunctional nano-carriers [123].

With these properties in mind, Neuman and co-workers carried out proof of concept studies demonstrating that CdSe/ZnS core/shell QDs photosensitize NO release from CrONO in aqueous solutions (Fig. 17) [119, 122]. In these studies, the QD/CrONO conjugates were an electrostatic assembly of the cationic CrONO on the negatively charged surface of QDs, and subsequent work [124] noted a clear correlation between the quenching of the QD PL and the spectral overlap integral consistent with a Förster resonance energy transfer (FRET) mechanism for the sensitization of the photoreaction. The antenna effect was evident in the marked enhancement in the rate of the NO release (compared to CrONO alone) owing to the much greater absorptivity of the QD chromophore.

In recent communications, Tan et al. [125, 126] have described the fabrication of water-dispersible Mn^{2+}-doped ZnS QDs encapsulated by the polysaccharide chitosan and conjugated to the photoNORM Roussin's black salt anion

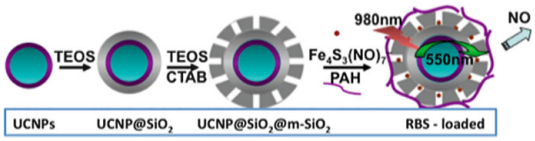

Fig. 18 Preparation UCNPs with a mesoporous silica shell impregnated with Roussin's Black Salt (*red dots*), a photo active nitric oxide generator, and coated with poly(allylamine). NIR irradiation leads to upconversion to wavelengths overlapping the RBS absorbance and NO uncaging [53]

$Fe_4S_3(NO)_7^-$ via electrostatic interaction. NIR excitation of these nanoparticles (20–140 nm diameters) with a 1,160 nm laser led to two-photon induced PL centered at 589 nm and labilization of NO from the RBS. At this stage it is not clear what is the functioning energy transfer mechanism for NO release.

Another approach to utilizing NIR light for effecting the photoreactions of visible or near-UV absorbing precursors of bioactive small molecules involves lanthanide ion-doped UCNPs [53, 127–129]. Since such UCNPs function via the sequential (rather than simultaneous) absorption of two or more NIR photons, a major advantage is that these can be activated using relatively inexpensive diode lasers rather than the pulsed lasers necessary with most TPE applications. For example, Yb^{3+}, Er^{3+}(or Tm^{3+})- doped $NaYF_4$ core-shell UCNPs will absorb 980 nm light to generate several visible wavelengths that can activate a photoNORM (or other small molecule precursors) as well as image the location of such conjugates. Thus, UCNPs have been shown to be effective sensitizers for NO release of several photoNORMs on the nanoparticle surface in a nano-carrier (Fig. 18) [80] as well as co-encapsulated in polymer composites [51, 130]. Such UCNP-containing materials offer very promising platform for the photochemical release bioactive small molecules at physiological sites, especially given that it has been demonstrated that UCNPs can be activated for NO release even when excited through tissue filters [51].

3 Carbon Monoxide Releasing Compounds

As discussed in Sect. 1, carbon monoxide is a natural product of mammalian physiology and various studies have linked exogenously applied to mechanisms of wound healing and inflammation suppression [25–40]. Notably, the mechanisms of these actions remain relatively unknown, although it seems likely that metal centers would be the most likely sites for reaction with CO. Here will be summarized recent studies concerned with the design of better and more versatile systems as photo-activated CO releasing moieties (photoCORMs), most of which are metal

carbonyl complexes. Special attention will be directed to the growing interest in developing multifunctional photo-activated pharmaceuticals [131–133].

3.1 Challenges Associated with Designing PhotoCORMs

Designing a novel photochemical pharmaceutical presents many challenges, most of which are relevant to design of an "ideal" photoCORM. To work well as a photochemical pharmaceutical agent, an ideal photoCORM should exhibit properties desirable to other photochemical small molecule releaser [118]. Most importantly, since these are to serve as benign reservoirs until activated, they should be stable in the dark and only release CO upon irradiation with the appropriate wavelength. Also, these should be biologically compatible—soluble in the appropriate delivery medium, relatively stable in an aqueous, aerobic environment, and non-toxic. Furthermore, the remaining molecular byproduct(s) of photochemical CO release (termed "iCORM") (Eq. 6) should not display undesired or unanticipated toxicity [134].

$$\mathrm{ML}_x(\mathrm{CO})_y \xrightarrow{h\nu} \mathrm{ML}_x(\mathrm{CO})_{y-z} + z\mathrm{CO} \tag{6}$$

In addition, for many applications a photoCORM would be most effective if CO release was enabled at longer visible wavelengths or in the NIR region (700–1,000 nm), where light has the greatest transmission through physiological fluids and tissue [135]. The most straightforward way to achieve this is by simply red-shifting the photoCORM absorbance; however, the photodissociation of CO from metal carbonyl complexes is notoriously wavelength-dependent. CO photodissociation typically occurs from the ligand field (LF) excited states [136, 137], and these photoactive LF bands typically lie in the UV or near-UV for most metal carbonyls. The stronger and more easily tunable absorption and emission bands of CO containing metal complexes generally involve MLCT states. While, computation techniques such as TD-DFT clearly show that such designations are simplified, since there is considerable mixing of ES character [138], they still provide useful qualitative indications of the photochemical reactivity to be expected in designing a molecular system to give greater CO photolability [118, 139].

An additional issue to consider is the biological localization and delivery of these photoCORMs. Since CO itself diffuses readily through both aqueous and lipid environments, an effective photoCORM would best be directly applied to the site of interest via injection or an implant, or have some mechanism for targeting this site [140, 141]. An important tool in facilitating this localization is the use of multifunctional photoCORMs that provide an identifier tag that can be combined with imaging techniques to identify the fate and localization of both the photoCORMs and the iCORMs within biological systems. Being able to directly identify the photoCORM makes this type of proposed therapy more powerful

because identifying CO in vivo is significantly more difficult by comparison, although there have been some recent developments in this regard [142–144].

The majority of reported photoCORMs are based on transition metal complexes of group 6, 7, and 8, since these form stable metal carbonyls. Several reviews have discussed the state of photoCORM research [20, 139, 145–149], so the present review will discuss only some selected conventional photoCORMs, while emphasizing multifunctional photoCORMs with luminescent properties.

3.2 PhotoCORMs

3.2.1 PhotoCORMs Based on Group 6 Metals

$Na_3[W(CO)_5(TPPTS)]$: One early photoCORM study involved the complex ions $M(CO)_3(TPPTS)^{3-}$ (M = Cr, Mo, W, TPPTS = tris(sulfonatophenyl)phosphine trianion) [42]. The sodium salt of $W(CO)_5(TPPTS)^{3-}$ is water soluble due to the anionic tris(sulfonatophenyl) phosphine ligand and is stable in aerated media when kept in the dark. However, irradiating a deaerated (or aerated) aqueous solution containing this complex with near-UV light lead to the loss of one CO with high apparent quantum yields for CO labilization; $\Phi_{app} = 0.90$ for $\lambda_{irr} = 313$ nm; $\Phi_{app} = 0.6$ for $\lambda_{irr} = 405$ nm. In addition, the tungsten photoproduct $W(CO)_4(H_2O)(TPPTS)^{3-}$ is stable under deaerated conditions, although it does react very slowly under a CO atmosphere to regenerate the starting complex. However, in *aerated* media this photoproduct undergoes autoxidation to release an additional 1.2–1.6 equivalent of CO (Scheme 3). In this context, the initial photoproduct $W(CO)_4(H_2O)(TPPTS)^{3-}$ is a proCORM, stable until converted by oxidation to a more labile CO releasing moiety.

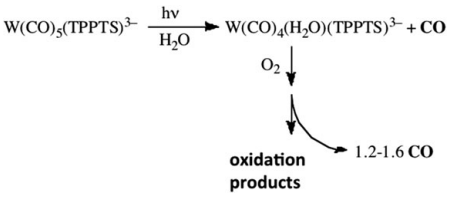

Scheme 3 Photoreactivity and subsequent CO release from $W(CO)_5(TPPTS)^{3-}$ in aerated aqueous solution.

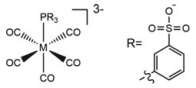

$M(CO)_5(TPPTS)^{3-}$ (M=Cr, Mo, W, TPPTS = tris(sulfonatophenyl)phosphine trianion)

The high quantum yield and biological compatibility of this complex suggest that it can be used in pharmaceutical applications; however, as with many such complexes, its electronic absorption spectrum is dominated by strong UV and near-UV ligand field bands. Since UV light has very poor tissue penetration, it could only be used in topical applications where shallow light activation could work. For applications involving internal applications, it is important to develop complexes that can be activated using longer wavelength light.

$M(CO)_4$(DPPQ): In an effort to promote stronger visible absorption bands and thermal stability in group 6 metal carbonyls, the bidentate P-N ligand diphenylphosphinoquinoline (DPPQ) (Pierri AE, unpublished results) was utilized. Neutral complexes of the type $M(CO)_4$(DPPQ) (M = Cr, Mo, W,) were found to meet these criteria with methanolic solutions displaying strong absorption bands in their visible spectra, 480 nm ($\varepsilon = 1.52 \times 10^3$ M^{-1} cm^{-1}), 452 nm (1.14×10^3 M^{-1} cm^{-1}), and 441 nm (1.30×10^3 M^{-1} cm^{-1}) for the Cr, Mo, and W complexes, respectively [145, 150]. In addition the ligand indeed lends thermal stability to the complex; aerated methanolic solutions of each were stable in the dark under ambient conditions. The highly hydrophobic nature of the DPPQ ligand unfortunately makes complexes of this type water-insoluble, although they are soluble in dimethylsulfoxide, which is commonly used as a drug delivery agent.

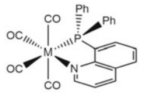

$M(CO)_4$(DPPQ)

The improved visible absorbance of this complex does indeed lead to photochemistry upon irradiation with longer wavelength visible light. For example, irradiating an aerobic methanolic solution of $Cr(CO)_4$(DPPQ) with $\lambda_{irr} = 355$, 366, 436, or 532 nm resulted in analogous spectral changes, namely, a decrease of all bands in the UV–vis region, as well as in the net release of four equivalents of CO. Thus, $Cr(CO)_4$(DPPQ) behaves similarly to the previously described $W(CO)_5(TPPTS)^{3-}$ in that it loses one CO photochemically with $\Phi_{app} = 0.10$ (for $\lambda_{irr} = 436$ nm), followed in aerated solution by oxidation of the first intermediate to release its full complement of COs, However, preliminary cell culture experiments suggested that $Cr(CO)_4$(DPPQ) may be too toxic to use as a photoCORM [150].

3.2.2 PhotoCORMs Based on Group 7 Metals

$Mn(CO)_3(R\text{-}tpm)^+$: Schatzschneider and co-workers [151] have reported a novel and versatile photoCORM platform based on manganese(I) tricarbonyl complexes with the tripodal ligand tris(pyrazolyl)methane (R-tpm): $(Mn(CO)_3(R\text{-}tpm)^+$. With R = H, this complex exhibits a strong absorption band centered ~360 nm ($\varepsilon = 2{,}080\ M^{-1}\ cm^{-1}$), and irradiation into this band liberates 1.9 equivalents of CO. An attractive aspect of this platform is that the acidic methyl proton can be replaced with a variety of different functional groups with minimal change to the photophysics, affording a multitude of functionalities from the same photoCORM backbone. An example of this functionalization is replacing the acidic proton with an ethoxypropargyl ether ($R = -CH_2OCH_2CCH$) which can serve as a linker to other pendants via the copper catalyzed azide-alkyne 1,3-dipolar cycloaddition ("click" reaction) or by Sonogashira coupling to aryl or vinyl halides. Using this attachment point, Schatzschneider and co-workers have been able to prepare the $Mn(CO)_3(R\text{-}tpm)^+$ photoCORMs with various pendant groups, from short peptide chains for use in biological targeting [152], to silica nanoparticles as a delivery vehicle [153], and to nano-diamonds for improved biocompatibility [154]. In each of these cases, the authors have been able to show that the photochemical properties of the $Mn(CO)_3(R\text{-}tpm)^+$ were retained regardless of the conjugation to the different pendants; upon exposure to UV light, all these constructs released CO.

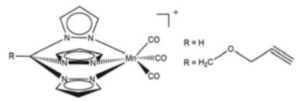

$Mn(CO)_3(R\text{-}tpm)$

$Mn(CO)_3(LLL)^+$: Expanding on Schatzschneider et al.'s studies with manganese carbonyls with tridentate amines, Gonzalez et al. reported a new class of Mn(I) photoCORMs with tripodal polypyridine ligands [155]. Complexes of the type $Mn(CO)_3(LLL)^+$ (LLL = tris(2-pyridyl)amine (tpa), *N*,*N*-bis(2-pyridylmethyl) amine (dpa) or (2-pyridylmethyl)(2-quinolylmethyl)amine (pqa)) showed broad UV centered absorption bands at 330 nm ($\varepsilon = 5.27 \times 10^3\ M^{-1}\ cm^{-1}$), 350 nm ($2.86 \times 10^3\ M^{-1}\ cm^{-1}$), and 360 nm ($6.06 \times 10^3\ M^{-1}\ cm^{-1}$) for acetonitrile solutions of tpa, dpa, and pqa complexes, respectively. These complexes appeared to be stable in dark aerated acetonitrile, but irradiation into the broad, near-UV absorption bands ($\lambda_{irr} = 358$ nm) resulted in CO photodissociation with the respective quantum yields 0.07 ± 0.01, 0.09 ± 0.01, and 0.06 ± 0.01.

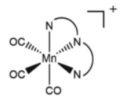

$Mn(CO)_3(LLL)^+$

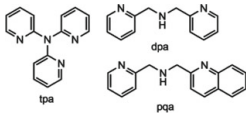

LLL

3.2.3 PhotoCORMs Based on Group 8 Metals

Norbornadiene iron(0) tricarbonyls: Lynam and co-workers [156] have reported a novel photoCORM based on iron norbornadiene complexes ($Fe(CO)_3$(norbornadiene-R2)), where modifying the ligand substituents tunes the CO release properties. In order to improve the thermal stability and the photochemical properties of the complex, methyl ester substituents were added at the 2- and 3-positions of the norbornadiene backbone. Unlike other norbornadiene iron carbonyl derivatives, tricarbonyl(η4-dimethylbicyclo[2.2.1]hepta-2,5-diene-2,3-dicarboxylate) iron(0) was found to be stable in the dark, although no comment was made regarding the stability in aerated media. Upon irradiation with 400 nm light, this complex undergoes CO photodissociation, resulting in the loss of two equivalents of CO. The authors also made efforts to determine the cellular toxicity of this complex by monitoring cell metabolism and assessing cell membrane damage. Concentrations of up to 140 μM showed no detectable damage to RAW264.7 cells, indicating that this complex shows no acute toxicity.

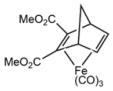

$Fe(CO)_3$(norbornadiene-R2)

3.3 Multifunctional PhotoCORMs for In Vivo Detection

Despite the knowledge that CO is tied to certain physiological responses, the chemistry surrounding its biological activity is not well understood owing in part to difficulties involved in detecting and measuring CO in cellular tissue [157]. In order to address this issue, various strategies for detection and visualization of CO in vivo are also being developed.

Two complimentary strategies may serve this application well. One approach involves developing photoCORMs that can be imaged directly using microscopy techniques. Another involves developing biologically compatible sensors for the detection of free CO. These two techniques could be used concurrently, giving information about the fate of the photoCORM and its iCORM, as well as the optimal location for CO delivery. Developing a technique that can give spatial and temporal information regarding the production of CO *inside* biological systems would provide an invaluable diagnostic tool that can help elucidate the role CO plays in human physiology. This, in turn, would provide guidelines for fine-tuning CO delivery methods to maximize their efficacy.

fac-**Re(bpy)$(CO)_3$$(tmp)^+$:** Rhenium(I) tricarbonyl complexes of the type Re(α-diimine)$(CO)_3X$ (X = Cl, Br) are typically stable in aerated media and are photoluminescent [158] but tend to be non-reactive toward photochemical substitution reactions [159]. The PL properties have found applications in vitro and in vivo imaging [160, 161]. Owing to an interest in using related compounds for photochemical CO_2 reduction Ishitani and co-workers [162] prepared complexes of the type *fac*-Re(bpy)$(CO)_3(PR_3)^+$, where the phosphine, because of its π-acidity renders the CO *trans* to it photolabile. Based upon these various observations, Antony et al. [163] were able to prepare a truly multifunctional rhenium complex that displayed a strong photoluminescence as well as CO photolability. This photoCORM was an air-stable and water-soluble variant of Ishitani's phosphine complexes, namely the salt *fac*-[Re(bpy)$(CO)_3$(tmp)]-(CF_3SO_3) (tmp = tris (hydroxymethyl)phosphine). The ligand tris(hydroxymethyl)phosphine (tmp) provided the additional benefit of conveying water-solubility to the complex. Irradiation ($\lambda_{irr} = 405$ nm) of this complex in aerated aqueous solution resulted in the loss of one equivalent of CO, and the production of an air-stable complex, presumably the solvento rhenium species Re(bpy)$(CO)_2(H_2O)^+$ (Eq. 7). A particularly remarkable feature of this system is that both the photoCORM and the rhenium product formed after photolysis display strong phosphorescence with respective PL λ_{max} values of 555 and 585 nm (Fig. 19). The quantum yield for emission from *fac*-Re (bpy)$(CO)_3(tmp)^+$ is 0.15 in ambient temperature aqueous solution.

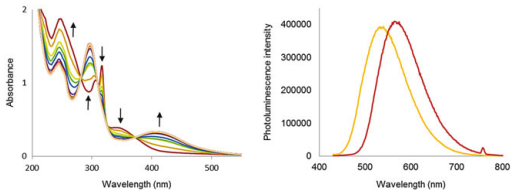

Fig. 19 *Left*: UV–visible spectral changes during photolysis $[Re(bpy)(CO)_3(thp)]^+$ in phosphate buffered saline solution at $\lambda = 405$ nm. *Right*, emission spectra before (*yellow*) and after (*red*) photolysis of $[Re(bpy)(CO)_3(thp)]^+$ ($\lambda_{irr} = 405$ nm)

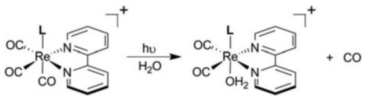

(7)

The optical spectrum of *fac*-$Re(bpy)(CO)_3(tmp)^+$ displays a MLCT centered at 345 nm ($\varepsilon = 3{,}500\ M^{-1}\ cm^{-1}$) that tails into the visible region (Fig. 19) enabling the photosubstitution reaction with 405 nm excitation. The initial interpretation is that the lowest triplet MLCT and LF excited states are close in energy, so MLCT excitation also leads to population of the substitution labile LF excited state, resulting in photochemical CO loss. Consistent with reports for similar compounds studied by Ishitani et al. [164], the quantum yield for CO dissociation increases with increasing temperature, which suggests that the photoreactive LF state is populated thermally. The quantum yields for CO photodissociation from *fac*-$Re(bpy)(CO)_3(tmp)^+$ was measured as 0.11 for $\lambda_{irr} = 405$ nm in ambient temperature aqueous solution.

This remarkable combination of luminescence and CO photolability makes this photoCORM attractive for in vitro imaging applications. Since *fac*-$Re(bpy)(CO)_3(tmp)^+$ and its photoproduct display different emission maxima, one can easily determine photoCORM uptake and localization inside cells, as well as CO release within cells by monitoring the emission shift for the transformation of the photoCORM to the iCORM. Using confocal microscopy, Antony et al. [163] were able to demonstrate the photoCORM uptake by PPC-1 cancer cells where it accumulates in the cytoplasm. No toxicity was observed up to 100 μM of the *fac*-$[Re(bpy)(CO)_3(tmp)](CF_3SO_3)$ salt. Upon irradiation with 405 nm light in the confocal microscope, the emission shift to longer wavelengths indicated that the solution phase photoreaction is indeed occurring inside the cells. Thus, the unique luminescent properties of this photoCORM provide a truly multifunctional platform that can both deliver CO photochemically and provide information regarding the

spatial and temporal release of CO. However, the obvious limitation to this system is the relatively high energy light needed to effect the photoreaction.

Xanthene-9-carboxylic acid: In 2013, Klán and co-workers reported a novel multifunctional photoCORM based on a fluorescein derivative that also has dual emissive and CO release properties [164]. In the dark, this water-soluble, air-stable compound is stable for up to a month in an aerated aqueous solution, making it ideal for biological applications. Additionally, this photoCORM, 6-hydroxy-3-oxo-3H-xanthene-9-carboxylic acid, has a strong visible absorbance ($\lambda = 488$ nm, $\varepsilon = \sim 1.8 \times 10^4\ M^{-1}\ cm^{-1}$) and a high fluorescence quantum yield ($\lambda_{em} = 530$ nm, $\Phi_{em} = 0.39$) suitable for in vitro imaging. Irradiation with 500 nm light leads to decarbonylation via a α-lactone intermediate, leading to a loss of one equivalent of CO and an isolable iCORM (Eq. 8). This photochemical process has a relatively small quantum towards CO loss of 6.8×10^{-4} in phosphate buffer at pH 7.4, but given the very high extinction coefficient, it is photoactive even at low power irradiation.

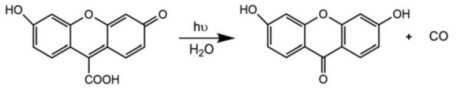

(8)

Unsaturated cyclic α-diketones: Another multifunctional organic photoCORM was reported by Kabanov et al. [165], who described the photodissociation of CO from cyclic α-diketones, where the fluorescent photoproduct (anthracene) may be used for imagining. These researchers designed a series of compounds based on anthracene derivatives with varying side chains to tune the hydrophobicity of the photoCORM. A short PEG group decreased the hydrophobicity, and a short alkyl chain increased the hydrophobicity (Eq. 9). This backbone was chosen because the anthracene has less acute toxicity, than most other polyaromatic hydrocarbons. Additionally, the well-known fluorescence of anthracene ($\Phi_{em} = 0.36$) provides the opportunity for cellular imagining after CO release. These compounds exhibit a broad *n*-π* absorption band centered around 465 nm, and irradiation into this band ($\lambda_{irr} = 470$ nm, extinction coefficients not reported) leads to the generation of two equivalents of CO, regardless of the side chains. This photochemistry was solvent insensitive, with the exception of water, where a solution of the PEG-functionalized compound in 1% DMSO/water exhibited no absorption band at 465 nm, nor any photochemistry upon irradiation, owing to the likely formation of ketone hydrates.

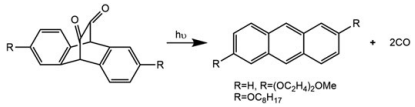

(9)

In order to protect the photoCORMs from ketone hydration, the derivatives were encapsulated in Pluronic 127 micelles—a biocompatible block copolymer with

polyethylene and polypropylene oxides commonly used for drug delivery [166]. The micelle interior is highly hydrophobic, enabling both the PEG- and alkyl-functionalized photoCORMs to be incorporated. These photoCORM loaded micelles were soluble in water, and retained their photoactivity, indicating that they were somewhat protected from hydration. Upon irradiation with 470 nm light, the encapsulated photoCORMs released CO with high yields (71–90%, depending on the side chains). To assess the biological compatibility of this multifunctional photoCORM, Pluronic micelles loaded with the hydrophobic diketone ($R{=}OC_8H_{17}$) were incubated with acute myeloid leukemia cells (KG-1) and no toxicity was detected up to 40 μM. Upon irradiation with 470 nm light and subsequent fluorescence microscopy, the blue emission from anthracene was observed in the treated cells, and they continued to proliferate normally after irradiation, suggesting that neither the micelle, nor any photoproduct was toxic to cells.

3.4 In Vivo Detection of CO

An important experimental challenge to understanding the biological activity is to obtain spatial and temporal information on how CO is produced and behaves inside living cells. In order to address this challenge, two groups have independently reported "turn-on" luminescent sensors for determining CO inside of living cells [143, 144]. Although still in early stages, such research into CO detectors should provide the foundation of what is likely to become an important tool for elucidating the roles CO plays in mammalian physiology.

COSer, a protein-based biosensor: In 2012, He and co-workers reported a novel CO-sensitive biosensor (COSer) based on the heme-containing protein CooA, a dimeric CO-sensing protein found in *Rhodospirillum rubrum* [144]. In the normal protein, CO selectively binds to the reduced (Fe^{II}) heme center of this protein, displacing a proline ligand, which, in turn, triggers a conformational change in the long C helix. To take advantage of this change, a fluorescent protein sensitive to conformational changes (a circularly permuted variant of yellow fluorescent protein, cpVenus) was inserted into the C helix (Fig. 20). Upon treating with 10 μM CO, COSer showed a twofold increased in emission ($\lambda_{em} = 528$ nm), a much larger increase than what was observed for other potentially competitive ligands: O_2 (100 μM), NO (20 μM), CN^- (100 μM), imidazole (100 μM), H_2S (excess), and GSH (excess), indicating that COSer is indeed selective for CO. Calibration curves were generated for COSer, meaning that it can serve as an incremental sensor, and a theoretical limit of detection was found to be between 1 and 2 μM CO.

To determine the efficacy of COSer in living cells, HeLa cells transfected with the COSer-containing expression vector were used as control experiments. COSer was found to be non-reactive towards a variety of typically encountered small molecules in vivo: O_2, NO, Na_2S, and GSH, but highly reactive towards CO. Detection was performed in two ways. In the first, addition of a saturated CO

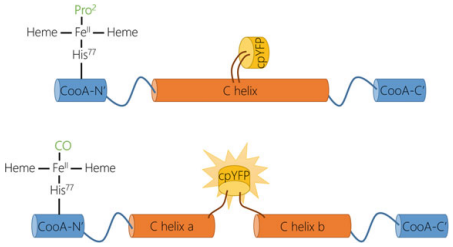

Fig. 20 Diagram depicting COSer binding to CO. Upon binding to CO, the C helix of CooA breaks in two ("C helix a" and "C helix b"). The *yellow* fluorescent protein (cpYFP) is inserted just at this breaking point, so that upon CO binding, cpYFP undergoes a conformational change, increasing its emission

solution elicited a response with 5 μM. Alternatively, a thermal-releasing CORM was added to mimic endogenous CO production, and this approach generated a measurable response with 1 μM CO. This novel CO sensor shows great promise as an in vivo tool in that its quick reaction times can provide temporal as well as spatial information on CO generation. However, the low signal to noise ratio (COSer only has a twofold increase in emission) may prove limiting.

COP-1, a palladium-based CO selective probe: In 2013, Michel et al. [143] reported a novel turn-on probe for CO detection based on well-known palladium carbonylation chemistry. They synthesized a palladium dimeric complex (COP-1), a modified boron dipyrromethane difluoride (BODIPY) core fluorescent dye as a ligand. While coordinated to palladium, the BODIPY fluorescence is quenched through spin-orbit coupling. However, reaction with CO in aqueous media leads to the carboxylation of the Pd–C bond and reduced Pd^0 (Eq. 10). Release of the BODIPY derivatized ligand from the Pd results in a strong fluorescence. In Dulbecco's phosphate buffered saline (DPBS, pH 7.4), COP-1 displays a weak emission ($\lambda_{em} = 503$ nm, $\Phi = 0.01$), but exposure to a thermal-releasing CORM ($Ru(CO)_3Cl(glycinate)$ [38]) leads to the formation of the fluorescent carbonylation product ($\lambda_{max} = 499$ nm, $\varepsilon = 2.3 \times 10^4$ M^{-1} cm^{-1}, $\lambda_{em} = 507$ nm, $\Phi = 0.44$) over the course of 60 min. With increasing CO concentration, they observed incremental fluorescence increases, with a tenfold increase maximum and a detection limit of approximately 1 μM.

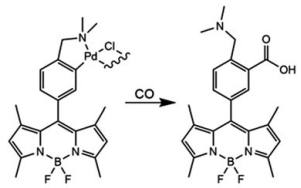

(10)

COP-1.

COP-1 was shown to have excellent specificity towards CO due to its very specific reactivity: other biologically relevant reactive species, such as H_2O_2, *t*BuOOH, OCl^-, O_2^-, NO, $ONOO^-$, and H_2S failed to produce the same fluorescence response as CO. This probe also found to work well as an in vitro sensor. COP-1 incubated with HEK293T cells was found to be non-toxic up to 10 μM and stable (non-emissive) for a period of 30 min. Co-incubating COP-1 (1 μM) with the CORM (5 μM) resulted in a detectable emission increase in the cells after 45 min monitored by confocal microscopy. This probe seems to be well suited for in vivo detection of CO because it exhibits a highly selective robust turn-on indicator for CO with low detection limits, and the absence of cellular toxicity under the working concentrations.

Summary, Conclusions, Outlook

We have summarized here the studies from a growing number of laboratories into the delivery of the bioactive small molecules nitric oxide and carbon monoxide to physiological targets using light as a trigger for uncaging. Photochemical activation of the prodrug corresponds to a very promising technique since one is able to control timing and location. Furthermore, since the concentration of agents like NO and CO dramatically affects the biological response, it is extremely important to be able to control the dosage of these molecules. The fact that the extent of a photochemical reaction is generally directly proportional to the amount of light absorbed by the photoNORM or photoCORM provides control of such dosing. A number of different systems based on metal-coordination and organometallic complexes were described. We have also discussed efforts to design some molecular species as well as conjugates that allow one to image the delivery site, and this will be a focus of continuing studies of caged NO and CO. A really interesting example is the nanoplatform for dual-color fluorescent, bimodal phototherapy described by Sortino and co-workers [166] that not only can be imaged via PL but also generates both NO and singlet oxygen when subjected

(continued)

to blue light. Also emphasized in our discussion were efforts to facilitate NO or CO uncaging using long visible range or near infrared excitation wavelengths, since these will be more effective in penetrating tissue than blue or near-UV wavelengths. Such attempts have taken two directions, one being molecular design that shifts the excited states reactive toward the uncaging process to lower energies, the other being the design of conjugate systems that utilize photophysical multiphoton methods to access higher energy excited states with NIR light. We can look forward to very interesting continuing developments in these areas and anticipate the application of these systems for clinical delivery of CO and NO.

Acknowledgements This work was supported by a grant to PCF (CHE-1058794) from the US National Science Foundation, by a fellowship to AEP from the UCSB Partnership for International Research and Education in Electron Chemistry and Catalysis at Interfaces (NSF grant OISE-0968399).

References

1. Ignarro LJ (2010) Nitric oxide: biology and pathobiology, 2nd edn. Elsevier Inc., Burlington
2. Fukumura D, Kashiwagi S, Jain RK (2006) The role of nitric oxide in tumour progression. Nat Rev Cancer 6:521–534
3. Weiming X, Li Zhi L, Marilena Loizidou MA, Ian GC (2002) The role of nitric oxide in cancer. Cell Res 12:311–320
4. Katusic ZS (2007) Mechanisms of endothelial dysfunction induced by aging role of arginase I. Circ Res 101:640–641
5. Herrera MD, Mingorance C, Rodríguez-Rodríguez R, Alvarez de Sotomayor M (2010) Endothelial dysfunction and aging: an update. Ageing Res Rev 9:142–152
6. Ridnour LA, Thomas DD, Switzer C, Flores-Santana W, Isenberg JS, Ambs S, Roberts DD, Wink DA (2008) Molecular mechanisms for discrete nitric oxide levels in cancer. Nitric Oxide 19:73–76
7. Fukuto JM, Carrington SJ, Tantillo DJ, Harrison JG, Ignarro LJ, Freeman BA, Chen A, Wink DA (2012) Small molecule signaling agents: the integrated chemistry and biochemistry of nitrogen oxides, oxides of carbon, dioxygen, hydrogen sulfide, and their derived species. Chem Res Toxicol 25:769–793
8. Wu L, Wang R (2005) Carbon monoxide: endogenous production, physiological functions, and pharmacological applications. Pharmacol Rev 57:585–630
9. Vandiver MS, Snyder SH (2012) Hydrogen sulfide: a gasotransmitter of clinical relevance. J Mol Med 90:255–263
10. Frost MC, Reynolds MM, Meyerhoff ME (2005) Polymers incorporating nitric oxide releasing/generating substances for improved biocompatibility of blood-contacting medical devices. Biomaterials 26:1685–1693
11. Keefer LK (2003) Progress toward clinical application of the nitric oxide—releasing diazeniumdiolates. Annu Rev Pharmacol Toxicol 43:585–607
12. Schairer DO, Chouake JS, Nosanchuk JD, Friedman AJ (2012) The potential of nitric oxide releasing therapies as antimicrobial agents. Virulence 3:271

13. Carpenter AW, Schoenfisch MH (2012) Nitric oxide release: part II. Therapeutic applications. Chem Soc Rev 41:3742–3752
14. Ford P, Bourassa J, Miranda K, Lee B, Lorkovic I, Boggs S, Kudo S, Laverman L (1998) Photochemistry of metal nitrosyl complexes. Delivery of nitric oxide to biological targets. Coord Chem Rev 171:185–202
15. Sortino S (2010) Light-controlled nitric oxide delivering molecular assemblies. Chem Soc Rev 39:2903–2913
16. Ciesienski KL, Franz KJ (2011) Keys for unlocking photolabile metal-containing cages. Angew Chem Int Ed 50:814–824
17. DeLeo MA, Ford PC (2000) Photoreactions of coordinated nitrite ion. Reversible nitric oxide labilization from the chromium (III) complex [*trans*-Cr(cyclam)$(ONO)_2]^+$. Coord Chem Rev 208:47–59
18. Ostrowski AD, Absalonson RO, Leo MAD, Wu G, Pavlovich JG, Adamson J, Azhar B, Iretskii AV, Megson IL, Ford PC (2011) Photochemistry of *trans*-Cr(cyclam)$(ONO)_2^+$, a Nitric Oxide Precursor. Inorg. Chem. 50:4453-4462. Correction: (2011). Inorg Chem 50:5848
19. Ostrowski AD, Deakin SJ, Azhar B, Miller TW, Franco N, Cherney MM, Lee AJ, Burstyn JN, Fukuto JM, Megson IL (2009) Nitric oxide photogeneration from *trans*-Cr (cyclam)$(ONO)_2^+$ in a reducing environment. Activation of soluble guanylyl cyclase and arterial vasorelaxation. J Med Chem 53:715–722
20. Schatzschneider U (2010) Photoactivated biological activity of transition-metal complexes. Eur J Inorg Chem 2010:1451–1467
21. Bordini J, Ford PC, Tfouni E (2005) Photochemical release of nitric oxide from a regenerable, sol-gel encapsulated Ru–salen–nitrosyl complex. Chem Commun 4169–4171
22. Halpenny GM, Olmstead MM, Mascharak PK (2007) Incorporation of a designed ruthenium nitrosyl in PolyHEMA hydrogel and light-activated delivery of NO to myoglobin. Inorg Chem 46:6601–6606
23. Mitchell-Koch JT, Reed TM, Borovik A (2004) Light-activated transfer of nitric oxide from a porous material. Angew Chem 116:2866–2869
24. Sjöstrand T (1952) The formation of carbon monoxide by the decomposition of haemoglobin in vivo. Acta Physiol Scand 26:338–344
25. Maines MD (1992) Heme oxygenase: clinical applications and functions. CRC, Boca Raton
26. Heinemann SH, Hoshi T, Westerhausen M, Schiller A (2014) Carbon monoxide – physiology, detection and controlled release. Chem Commun 50:3644–3660
27. Verma A, Hirsch D, Glatt C, Ronnett G, Snyder S (1993) Carbon monoxide: a putative neural messenger. Science 259:381–384
28. Motterlini R, Gonzales A, Foresti R, Clark JE, Green CJ, Winslow RM (1998) Heme oxygenase-1–derived carbon monoxide contributes to the suppression of acute hypertensive responses in vivo. Circ Res 83:568–577
29. Choi AM, Otterbein LE (2002) Emerging role of carbon monoxide in physiologic and pathophysiologic states. Antioxid Redox Signal 4:227–228
30. Ryter SW, Alam J, Choi AM (2006) Heme oxygenase-1/carbon monoxide: from basic science to therapeutic applications. Physiol Rev 86:583–650
31. Otterbein LE (2002) Carbon monoxide: innovative anti-inflammatory properties of an age-old gas molecule. Antioxid Redox Signal 4:309–319
32. Nakao A, Kimizuka K, Stolz DB, Neto JS, Kaizu T, Choi AMK, Uchiyama T, Zuckerbraun BS, Nalesnik MA, Otterbein LE, Murase N (2003) Carbon monoxide inhalation protects rat intestinal grafts from ischemia/reperfusion injury. Am J Pathol 163:1587–1598
33. Tavares AFN, Teixeira M, Romão CC, Seixas JD, Nobre LS, Saraiva LM (2011) Reactive oxygen species mediate bactericidal killing elicited by carbon monoxide-releasing molecules. J Biol Chem 286:26708–26717
34. Kim HP, Ryter SW, Choi AMK (2006) CO as a cellular signaling molecule. Annu Rev Pharmacol Toxicol 46:411–449

35. Otterbein LE, Soares MP, Yamashita K, Bach FH (2003) Heme oxygenase-1: unleashing the protective properties of heme. Trends Immunol 24:449–455
36. Otterbein LE, Zuckerbraun BS, Haga M, Liu F, Song R, Usheva A, Stachulak C, Bodyak N, Smith RN, Csizmadia E, Tyagi S, Akamatsu Y, Flavell RJ, Billiar TR, Tzeng E, Bach FH, Choi AMK, Soares MP (2003) Carbon monoxide suppresses arteriosclerotic lesions associated with chronic graft rejection and with balloon injury. Nat Med 9:183–190
37. Akamatsu Y, Haga M, Tyagi S, Yamashita K, Graça-Souza AV, Ollinger R, Czismadia E, May GA, Ifedigbo E, Otterbein LE (2004) Heme oxygenase-1-derived carbon monoxide protects hearts from transplant associated ischemia reperfusion injury. FASEB J 18:771–772
38. Motterlini R, Clark JE, Foresti R, Sarathchandra P, Mann BE, Green CJ (2002) Carbon monoxide-releasing molecules characterization of biochemical and vascular activities. Circ Res 90:e17–e24
39. Johnson TR, Mann BE, Clark JE, Foresti R, Green CJ, Motterlini R (2003) Metal carbonyls: a new class of pharmaceuticals? Angew Chem Int Ed 42:3722–3729
40. Alberto R, Motterlini R (2007) Chemistry and biological activities of CO-releasing molecules (CORMs) and transition metal complexes. Dalton Trans 1651–1660
41. Mann B (2010) Carbon monoxide: an essential signalling molecule. In: Jaouen G, Metzler-Nolte N (eds) Medicinal organometallic chemistry. Springer, Heidelberg, pp 247–285
42. Rimmer RD, Richter H, Ford PC (2009) A photochemical precursor for carbon monoxide release in aerated aqueous media. Inorg Chem 49:1180–1185
43. König K (2006) Cell damage during multi-photon microscopy. In: Pawley JB (ed) Handbook of biological confocal microscopy. Springer, US, pp 680–689
44. Wecksler S, Mikhailovsky A, Ford PC (2004) Photochemical production of nitric oxide via two-photon excitation with NIR light. J Am Chem Soc 126:13566–13567
45. Wecksler SR, Mikhailovsky A, Korystov D, Ford PC (2006) A two-photon antenna for photochemical delivery of nitric oxide from a water-soluble, dye-derivatized iron nitrosyl complex using NIR light. J Am Chem Soc 128:3831–3837
46. Wecksler SR, Hutchinson J, Ford PC (2006) Toward development of water soluble dye derivatized nitrosyl compounds for photochemical delivery of NO. Inorg Chem 45:1192–1200
47. Wecksler SR, Mikhailovsky A, Korystov D, Buller F, Kannan R, Tan L-S, Ford PC (2007) - Single-and two-photon properties of a dye-derivatized Roussin's red salt ester ($Fe_2(\mu\text{-}RS)_2(NO)_4$) with a large TPA cross section. Inorg Chem 46:395–402
48. Eroy-Reveles AA, Leung Y, Beavers CM, Olmstead MM, Mascharak PK (2008) Near-infrared light activated release of nitric oxide from designed photoactive manganese nitrosyls: strategy, design, and potential as NO donors. J Am Chem Soc 130:4447–4458
49. Rose MJ, Mascharak PK (2009) Photosensitization of Ruthenium nitrosyls to red light with an isoelectronic series of heavy-atom chromophores: experimental and density functional theory studies on the effects of O-, S-and Se-substituted coordinated dyes. Inorg Chem 48:6904–6917
50. Heilman B, Mascharak PK (2013) Light-triggered nitric oxide delivery to malignant sites and infection. Philos Trans R Soc A 371:20120368
51. Burks PT, Garcia JV, GonzalezIrias R, Tillman JT, Niu M, Mikhailovsky AA, Zhang J, Zhang F, Ford PC (2013) Nitric oxide releasing materials triggered by near-infrared excitation through tissue filters. J Am Chem Soc 135:18145–18152
52. Nakagawa H, Hishikawa K, Eto K, Ieda N, Namikawa T, Kamada K, Suzuki T, Miyata N, J-i N (2013) Fine spatiotemporal control of nitric oxide release by infrared pulse-laser irradiation of a photolabile donor. ACS Chem Biol 8:2493–2500
53. Garcia JV, Zhang F, Ford PC (2013) Multi-photon excitation in uncaging the small molecule bioregulator nitric oxide. Philos Trans R Soc A 371:1995
54. DeRosa F, Bu X, Ford PC (2005) Chromium (III) complexes for photochemical nitric oxide generation from coordinated nitrite: synthesis and photochemistry of macrocyclic complexes with pendant chromophores, *trans*-$[Cr(L)(ONO)_2]BF_4$. Inorg Chem 44:4157–4165

55. De Leo M, Ford PC (1999) Reversible photolabilization of NO from chromium (III)-coordinated nitrite. A new strategy for nitric oxide delivery. J Am Chem Soc 121:1980–1981
56. Wagenknecht PS, Ford PC (2011) Metal centered ligand field excited states: their roles in the design and performance of transition metal based photochemical molecular devices. Coord Chem Rev 255:591–616
57. Ostrowski AD, Lin BF, Tirrell MV, Ford PC (2012) Liposome encapsulation of a photochemical NO precursor for controlled nitric oxide release and simultaneous fluorescence imaging. Mol Pharm 9:2950–2955
58. Suslick KS, Watson RA (1991) Photochemical reduction of nitrate and nitrite by manganese and iron porphyrins. Inorg Chem 30:912–919
59. Suslick KS, Bautista JF, Watson RA (1991) Metalloporphyrin photochemistry with matrix isolation. J Am Chem Soc 113:6111–6114
60. Hoshino M, Nagashima Y, Seki H, De Leo M, Ford PC (1998) Laser flash photolysis studies of nitritomanganese (III) tetraphenylporphyrin. Reactions of O_2, NO, and pyridine with manganese (II) tetraphenylporphyrin. Inorg Chem 37:2464–2469
61. Enemark J, Feltham R (1974) Principles of structure, bonding, and reactivity for metal nitrosyl complexes. Coord Chem Rev 13:339–406
62. Ford PC, Lorkovic IM (2002) Mechanistic aspects of the reactions of nitric oxide with transition-metal complexes. Chem Rev 102:993–1018
63. Rose MJ, Mascharak PK (2008) Photoactive ruthenium nitrosyls: effects of light and potential application as NO donors. Coord Chem Rev 252:2093–2114
64. Bordini J, Novaes D, Borissevitch I, Owens B, Ford P, Tfouni E (2008) Acidity and photolability of ruthenium salen nitrosyl and aquo complexes in aqueous solutions. Inorg Chim Acta 361:2252–2258
65. Hoffman-Luca CG, Eroy-Reveles AA, Alvarenga J, Mascharak PK (2009) Syntheses, structures, and photochemistry of manganese nitrosyls derived from designed Schiff base ligands: potential NO donors that can be activated by near-infrared light. Inorg Chem 48:9104–9111
66. Afshar RK, Patra AK, Olmstead MM, Mascharak PK (2004) Syntheses, structures, and reactivities of {Fe-NO} 6 nitrosyls derived from polypyridine-carboxamide ligands: photoactive NO-donors and reagents for S-nitrosylation of alkyl thiols. Inorg Chem 43:5736–5743
67. de Lima RG, Sauaia MG, Bonaventura D, Tedesco AC, Bendhack LM, da Silva RS (2006) Influence of ancillary ligand L in the nitric oxide photorelease by the $[Ru(L)(tpy)\ NO]^{3+}$ complex and its vasodilator activity based on visible light irradiation. Inorg Chim Acta 359:2543–2549
68. Ford P, Pereira J, Miranda K (2014) Mechanisms of nitric oxide reactions mediated by biologically relevant metal centers. In: Mingos DMP (ed) Nitrosyl complexes in inorganic chemistry, biochemistry and medicine II. Springer, Heidelberg, pp 99–135
69. Bates JN, Baker MT, Guerra R Jr, Harrison DG (1991) Nitric oxide generation from nitroprusside by vascular tissue: evidence that reduction of the nitroprusside anion and cyanide loss are required. Biochem Pharmacol 42:S157–S165
70. Kudo S, Bourassa JL, Boggs SE, Sato Y, Ford PC (1997) *In situ* nitric oxide (NO) measurement by modified electrodes: NO labilized by photolysis of metal nitrosyl complexes. Anal Biochem 247:193–202
71. Garino C, Salassa L (2013) The photochemistry of transition metal complexes using density functional theory. Philos Trans R Soc A 371:20120134
72. Flitney F, Megson I, Thomson JL, Kennovin G, Butler A (1996) Vasodilator responses of rat isolated tail artery enhanced by oxygen-dependent, photochemical release of nitric oxide from iron-sulphur-nitrosyls. Brit J Pharmacol 117:1549–1557
73. Bourassa J, DeGraff W, Kudo S, Wink DA, Mitchell JB, Ford PC (1997) Photochemistry of Roussin's Red Salt, $Na_2[Fe_2S_2(NO)_4]$, and of Roussin's Black Salt, $NH_4[Fe_4S_3(NO)_7]$. In situ nitric oxide generation to sensitize γ-radiation induced cell death. J Am Chem Soc 119:2853–2860

74. Mitchell JB, Wink DA, DeGraff W, Gamson J, Keefer LK, Krishna MC (1993) Hypoxic mammalian cell radiosensitization by nitric oxide. Cancer Res 53:5845–5848
75. Bourassa JL, Ford PC (2000) Flash and continuous photolysis studies of Roussin's red salt dianion $Fe_2S_2(NO)_4^{2-}$ in solution. Coord Chem Rev 200:887–900
76. Conrado CL, Wecksler S, Egler C, Magde D, Ford PC (2004) Synthesis and photochemical properties of a novel iron-sulfur-nitrosyl cluster derivatized with the pendant chromophore protoporphyrin IX. Inorg Chem 43:5543–5549
77. Conrado CL, Bourassa JL, Egler C, Wecksler S, Ford PC (2003) Photochemical investigation of Roussin's Red Salt Esters: $Fe_2(\mu\text{-}SR)_2(NO)_4$. Inorg Chem 42:2288–2293
78. Zheng Q, Bonoiu A, Ohulchanskyy TY, He GS, Prasad PN (2008) Water-soluble two-photon absorbing nitrosyl complex for light-activated therapy through nitric oxide release. Mol Pharm 5:389–398
79. Gouterman M, Khalil G-E (1974) Porphyrin free base phosphorescence. J Mol Spectrosc 53:88–100
80. Garcia JV, Yang J, Shen D, Yao C, Li X, Wang R, Stucky GD, Zhao D, Ford PC, Zhang F (2012) NIR-triggered release of caged nitric oxide using upconverting nanostructured materials. Small 8:3800–3805
81. Patra AK, Rowland JM, Marlin DS, Bill E, Olmstead MM, Mascharak PK (2003) Iron nitrosyls of a pentadentate ligand containing a single carboxamide group: syntheses, structures, electronic properties, and photolability of NO. Inorg Chem 42:6812–6823
82. Patra AK, Afshar R, Olmstead MM, Mascharak PK (2002) The first non-heme iron (III) complex with a ligated carboxamido group that exhibits photolability of a bound NO ligand. Angew Chem 114:2622–2625
83. Ghosh K, Eroy-Reveles AA, Avila B, Holman TR, Olmstead MM, Mascharak PK (2004) Reactions of NO with Mn (II) and Mn (III) centers coordinated to carboxamido nitrogen: synthesis of a manganese nitrosyl with photolabile NO. Inorg Chem 43:2988–2997
84. Merkle AC, Fry NL, Mascharak PK, Lehnert N (2011) Mechanism of NO photodissociation in photolabile manganese–NO complexes with pentadentate N_5 ligands. Inorg Chem 50:12192–12203
85. Hitomi Y, Iwamoto Y, Kodera M (2014) Electronic tuning of nitric oxide release from manganese nitrosyl complexes by visible light irradiation: enhancement of nitric oxide release efficiency by the nitro-substituted quinoline ligand. Dalton Trans 43:2161–2167
86. Eroy-Reveles AA, Leung Y, Mascharak PK (2006) Release of nitric oxide from a sol-gel hybrid material containing a photoactive manganese nitrosyl upon illumination with visible light. J Am Chem Soc 128:7166–7167
87. Frasconi M, Liu Z, Lei J, Wu Y, Strekalova E, Malin D, Ambrogio MW, Chen X, Botros YY, Cryns VL (2013) Photoexpulsion of surface-grafted ruthenium complexes and subsequent release of cytotoxic cargos to cancer cells from mesoporous silica nanoparticles. J Am Chem Soc 135:11603–11613
88. Howerton BS, Heidary DK, Glazer EC (2012) Strained ruthenium complexes are potent light-activated anticancer agents. J Am Chem Soc 134:8324–8327
89. Baranoff E, Collin J-P, Flamigni L, Sauvage J-P (2004) From ruthenium (II) to iridium (III): 15 years of triads based on bis-terpyridine complexes. Chem Soc Rev 33:147–155
90. Fry NL, Mascharak PK (2011) Photoactive ruthenium nitrosyls as NO donors: how to sensitize them toward visible light. Acc Chem Res 44:289–298
91. Bordini J, Hughes DL, Da Motta Neto JD, Jorge da Cunha C (2002) Nitric oxide photorelease from ruthenium salen complexes in aqueous and organic solutions. Inorg Chem 41:5410–5416
92. Carlos RM, Ferro AA, Silva HA, Gomes MG, Borges SS, Ford PC, Tfouni E, Franco DW (2004) Photochemical reactions of *trans*-$[Ru(NH_3)_4L(NO)]^{3+}$ complexes. Inorg Chim Acta 357:1381–1388

93. Paula Q, Batista A, Castellano E, Ellena J (2002) On the lability of dimethylsulfoxide (DMSO) coordinated to the $\{Ru^{II}\text{-}NO^{+}\}$ species: X-ray structures of *mer*-$[RuCl_3(DMSO)_2NO)]$ and *mer*-$[RuCl_3(CD_3CN)(DMSO)(NO)]$. J Inorg Biochem 90:144–148
94. Miranda KM, Bu X, Lorkovic I, Ford PC (1997) Synthesis and structural characterization of several ruthenium porphyrin nitrosyl complexes. Inorg Chem 36:4838–4848
95. Tfouni E, Doro FG, Figueiredo LE, Pereira JC, Metzker G, Franco DW (2010) Tailoring NO donors metallopharmaceuticals: ruthenium nitrosyl ammines and aliphatic tetraazamacrocycles. Curr Med Chem 17:3643–3657
96. Oliveira FS, Togniolo V, Pupo TT, Tedesco AC, da Silva RS (2004) Nitrosyl ruthenium complex as nitric oxide delivery agent: synthesis, characterization and photochemical properties. Inorg Chem Commun 7:160–164
97. Sauaia MG, de Lima RG, Tedesco AC, da Silva RS (2003) Photoinduced NO release by visible light irradiation from pyrazine-bridged nitrosyl ruthenium complexes. J Am Chem Soc 125:14718–14719
98. Marquele-Oliveira F, de Almeida Santana DC, Taveira SF, Vermeulen DM, Moraes de Oliveira AR, da Silva RS, Lopez RFV (2010) Development of nitrosyl ruthenium complex-loaded lipid carriers for topical administration: improvement in skin stability and in nitric oxide release by visible light irradiation. J Pharm Biomed Anal 53:843–851
99. Works CF, Jocher CJ, Bart GD, Bu X, Ford PC (2002) Photochemical nitric oxide precursors: synthesis, photochemistry, and ligand substitution kinetics of ruthenium salen nitrosyl and ruthenium salophen nitrosyl complexes. Inorg Chem 41:3728–3739
100. Tfouni E, Krieger M, McGarvey BR, Franco DW (2003) Structure, chemical and photochemical reactivity and biological activity of some ruthenium amine nitrosyl complexes. Coord Chem Rev 236:57–69
101. Lorkovic IM, Miranda KM, Lee B, Bernhard S, Schoonover JR, Ford PC (1998) Flash photolysis studies of the ruthenium (II) porphyrins Ru (P)(NO)(ONO). Multiple pathways involving reactions of intermediates with nitric oxide. J Am Chem Soc 120:11674–11683
102. Oliveira FS, Ferreira KQ, Bonaventura D, Bendhack LM, Tedesco AC, Machado SP, Tfouni E, Silva RSD (2007) The macrocyclic effect and vasodilation response based on the photoinduced nitric oxide release from *trans*-$[RuCl(tetraazamacrocycle)\ NO]^{2+}$. J Inorg Biochem 101:313–320
103. Ford PC, Wecksler S (2005) Photochemical reactions leading to NO and NO_x generation. Coord Chem Rev 249:1382–1395
104. Ford PC, Laverman LE (2005) Reaction mechanisms relevant to the formation of iron and ruthenium nitric oxide complexes. Coord Chem Rev 249:391–403
105. Rose MJ, Olmstead MM, Mascharak PK (2007) Photoactive ruthenium nitrosyls derived from quinoline-and pyridine-based ligands: accelerated photorelease of NO due to quinoline ligation. Polyhedron 26:4713–4718
106. Patra AK, Mascharak PK (2003) A ruthenium nitrosyl that rapidly delivers NO to proteins in aqueous solution upon short exposure to UV light. Inorg Chem 42:7363–7365
107. Fry NL, Heilman BJ, Mascharak PK (2010) Dye-tethered ruthenium nitrosyls containing planar dicarboxamide tetradentate N_4 ligands: effects of in-plane ligand twist on NO photolability. Inorg Chem 50:317–324
108. Patra AK, Rose MJ, Murphy KA, Olmstead MM, Mascharak PK (2004) Photolabile ruthenium nitrosyls with planar dicarboxamide tetradentate N4 ligands: effects of in-plane and axial ligand strength on NO release. Inorg Chem 43:4487–4495
109. Welbes LL, Borovik A (2005) Confinement of metal complexes within porous hosts: development of functional materials for gas binding and catalysis. Acc Chem Res 38:765–774
110. Robbins ME, Schoenfisch MH (2003) Surface-localized release of nitric oxide via sol-gel chemistry. J Am Chem Soc 125:6068–6069

111. Heilman BJ, St. John J, Oliver SR, Mascharak PK (2012) Light-triggered eradication of acinetobacter baumannii by means of NO delivery from a porous material with an entrapped metal nitrosyl. J Am Chem Soc 134:11573–11582
112. Halpenny GM, Gandhi KR, Mascharak PK (2010) Eradication of pathogenic bacteria by remote delivery of NO via light triggering of nitrosyl-containing materials. ACS Med Chem Lett 1:180–183
113. Halpenny GM, Steinhardt RC, Okialda KA, Mascharak PK (2009) Characterization of pHEMA-based hydrogels that exhibit light-induced bactericidal effect via release of NO. J Mater Sci Mater Med 20:2353–2360
114. Bohlender C, Landfester K, Crespy D, Schiller A (2013) Unconventional non-aqueous emulsions for the encapsulation of a phototriggerable NO-donor complex in polymer nanoparticles. Part Part Syst Char 30:138–142
115. Heilman BJ, Halpenny GM, Mascharak PK (2011) Synthesis, characterization, and light–controlled antibiotic application of a composite material derived from polyurethane and silica xerogel with embedded photoactive manganese nitrosyl. J Biomed Mater Res Part B Appl Biomater 99:328–337
116. Ford PC (2013) Photochemical delivery of nitric oxide. Nitric Oxide 34:56–64
117. Ostrowski AD, Ford PC (2009) Metal complexes as photochemical nitric oxide precursors: potential applications in the treatment of tumors. Dalton Trans 10660–10669
118. Ford PC (2008) Polychromophoric metal complexes for generating the bioregulatory agent nitric oxide by single-and two-photon excitation. Acc Chem Res 41:190–200
119. Neuman D, Ostrowski AD, Absalonson RO, Strouse GF, Ford PC (2007) Photosensitized NO release from water-soluble nanoparticle assemblies. J Am Chem Soc 129:4146–4147
120. Rose MJ, Fry NL, Marlow R, Hinck L, Mascharak PK (2008) Sensitization of ruthenium nitrosyls to visible light via direct coordination of the dye resorufin: trackable NO donors for light-triggered NO delivery to cellular targets. J Am Chem Soc 130:8834–8846
121. Fry NL, Wei J, Mascharak PK (2011) Triggered dye release via photodissociation of nitric oxide from designed ruthenium nitrosyls: turn-ON fluorescence signaling of nitric oxide delivery. Inorg Chem 50:9045–9052
122. Neuman D, Ostrowski AD, Mikhailovsky AA, Absalonson RO, Strouse GF, Ford PC (2008) Quantum dot fluorescence quenching pathways with Cr(III) complexes. Photosensitized NO production from *trans*-Cr(cyclam)$(ONO)_2^+$. J Am Chem Soc 130:168–175
123. Algar WR, Kim H, Medintz IL, Hildebrandt N (2014) Emerging non-traditional Förster resonance energy transfer configurations with semiconductor quantum dots: investigations and applications. Coord Chem Rev 263:65–85
124. Burks PT, Ostrowski AD, Mikhailovsky AA, Chan EM, Wagenknecht PS, Ford PC (2012) Quantum dot photoluminescence quenching by Cr (III) complexes. Photosensitized reactions and evidence for a FRET mechanism. J Am Chem Soc 134:13266–13275
125. Tan L, Wan A, Zhu X, Li H (2014) Nitric oxide release triggered by two-photon excited photoluminescence of engineered nanomaterials. Chem Commun 50:5725–5728
126. Tan L, Wan A, Zhu X, Li H (2014) Visible light-triggered nitric oxide release from near-infrared fluorescent nanospheric vehicles. Analyst 139:3398–3406
127. Chan EM, Han G, Goldberg JD, Gargas DJ, Ostrowski AD, Schuck PJ, Cohen BE, Milliron DJ (2012) Combinatorial discovery of lanthanide-doped nanocrystals with spectrally pure upconverted emission. Nano Lett 12:3839–3845
128. Chen G, Qiu H, Prasad PN, Chen X (2014) Upconversion nanoparticles: design, nanochemistry, and applications in theranostics. Chem Rev 114:5161–5214
129. Liu Y, Tu D, Zhu H, Chen X (2013) Lanthanide-doped luminescent nanoprobes: controlled synthesis, optical spectroscopy, and bioapplications. Chem Soc Rev 42:6924–6958
130. Mase JD, Razgoniaev AO, Tschirhart MK, Ostrowski AD (2014) Light-controlled release of nitric oxide from solid polymer composite materials using visible and near infra-red light (submitted)

131. Sun B, Ranganathan B, Feng S-S (2008) Multifunctional poly (D,L-lactide-*co*-glycolide)/montmorillonite (PLGA/MMT) nanoparticles decorated by Trastuzumab for targeted chemotherapy of breast cancer. Biomaterials 29:475–486
132. Nasongkla N, Bey E, Ren J, Ai H, Khemtong C, Guthi JS, Chin S-F, Sherry AD, Boothman DA, Gao J (2006) Multifunctional polymeric micelles as cancer-targeted, MRI-ultrasensitive drug delivery systems. Nano Lett 6:2427–2430
133. Torchilin VP (2012) Multifunctional nanocarriers. Adv Drug Deliver Rev 64(Suppl):302–315
134. Motterlini R, Sawle P, Hammad J, Bains S, Alberto R, Foresti R, Green CJ (2005) CORM-A1: a new pharmacologically active carbon monoxide-releasing molecule. FASEB J 19:284–286
135. König K (2000) Multiphoton microscopy in life sciences. J Microsc 200:83–104
136. Geoffrey GL, Wrighton ML (1979) Organometallic photochemistry. Elsevier, New York
137. Wrighton M (1974) Photochemistry of metal carbonyls. Chem Rev 74:401–430
138. Záliš S, Milne CJ, El Nahhas A, Blanco-Rodríguez AM, van der Veen RM, Vlcek A Jr (2013) Re and Br X-ray absorption near-edge structure study of the ground and excited states of $[ReBr(CO)_3(bpy)]$ interpreted by DFT and TD-DFT calculations. Inorg Chem 52:5775–5785
139. Schatzschneider U (2011) PhotoCORMs: light-triggered release of carbon monoxide from the coordination sphere of transition metal complexes for biological applications. Inorg Chim Acta 374:19–23
140. Gao X, Cui Y, Levenson RM, Chung LW, Nie S (2004) In vivo cancer targeting and imaging with semiconductor quantum dots. Nat Biotechnol 22:969–976
141. Brannon-Peppas L, Blanchette JO (2012) Nanoparticle and targeted systems for cancer therapy. Adv Drug Deliver Rev 64:206–212
142. Yuan L, Lin W, Tan L, Zheng K, Huang W (2013) Lighting up carbon monoxide: fluorescent probes for monitoring CO in living cells. Angew Chem Int Ed 52:1628–1630
143. Michel BW, Lippert AR, Chang CJ (2012) A reaction-based fluorescent probe for selective imaging of carbon monoxide in living cells using a palladium-mediated carbonylation. J Am Chem Soc 134:15668–15671
144. Wang J, Karpus J, Zhao BS, Luo Z, Chen PR, He C (2012) A selective fluorescent probe for carbon monoxide imaging in living cells. Angew Chem 124:9790–9794
145. Rimmer RD, Pierri AE, Ford PC (2012) Photochemically activated carbon monoxide release for biological targets. Toward developing air-stable photoCORMs labilized by visible light. Coord Chem Rev 256:1509–1519
146. Gonzales MA, Mascharak PK (2014) Photoactive metal carbonyl complexes as potential agents for targeted CO delivery. J Inorg Biochem 133:127–135
147. Romao CC, Blattler WA, Seixas JD, Bernardes GJL (2012) Developing drug molecules for therapy with carbon monoxide. Chem Soc Rev 41:3571–3583
148. Simpson PV, Schatzschneider U (2014) Release of bioactive molecules using metal complexes. Inorganic chemical biology: principles, techniques and applications. Wiley, West Sussex, pp 309–339.
149. Knebel WJ, Angelici RJ (1973) Phosphorus-nitrogen donor ligand complexes of chromium, molybdenum and tungsten carbonyls. Inorg Chim Acta 7:713–716
150. Niesel J, Pinto A, N'Dongo HWP, Merz K, Ott I, Gust R, Schatzschneider U (2008) Photoinduced CO release, cellular uptake and cytotoxicity of a tris(pyrazolyl)methane (tpm) manganese tricarbonyl complex. Chem Commun 1798–1800
151. Pfeiffer H, Rojas A, Niesel J, Schatzschneider U (2009) Sonogashira and "Click" reactions for the -terminal and side-chain functionalization of peptides with $[Mn(CO)_3(tpm)]^+$-based CO releasing molecules (tpm= tris(pyrazolyl)methane). Dalton Trans 4292–4298
152. Dördelmann G, Pfeiffer H, Birkner A, Schatzschneider U (2011) Silicium dioxide nanoparticles as carriers for photoactivatable CO-releasing molecules (PhotoCORMs). Inorg Chem 50:4362–4367

153. Dördelmann G, Meinhardt T, Sowik T, Krueger A, Schatzschneider U (2012) CuAAC click functionalization of azide-modified nanodiamond with a photoactivatable CO-releasing molecule (PhotoCORM) based on $[Mn(CO)_3(tpm)]^+$. Chem Commun 48:11528–11530
154. Gonzalez MA, Yim MA, Cheng S, Moyes A, Hobbs AJ, Mascharak PK (2011) Manganese carbonyls bearing tripodal polypyridine ligands as photoactive carbon monoxide-releasing molecules. Inorg Chem 51:601–608
155. Atkin AJ, Fairlamb IJS, Ward JS, Lynam JM (2012) CO Release from norbornadiene iron (0) tricarbonyl complexes: importance of ligand dissociation. Organometallics 31:5894–5902
156. Foresti R, Bani-Hani MG, Motterlini R (2008) Use of carbon monoxide as a therapeutic agent: promises and challenges. Intens Care Med 34:649–658
157. Klein A, Vogler C, Kaim W (1996) The δ in 18+ δ electron complexes: importance of the metal/ligand interface for the substitutional reactivity of "Re (0)" complexes(α-diimine-) ReI $(CO)_3(X)$. Organometallics 15:236–244
158. Hori H, Koike K, Ishizuka M, Takeuchi K, Ibusuki T, Ishitani O (1997) Preparation and characterization of $[Re(bpy)(CO)_3L][SbF_6]$(L= phosphine, phosphite). J Organomet Chem 530:169–176
159. Lo KK-W, Louie M-W, Zhang KY (2010) Design of luminescent iridium (III) and rhenium (I) polypyridine complexes as *in vitro* and *in vivo* ion, molecular and biological probes. Coord Chem Rev 254:2603–2622
160. Amoroso AJ, Coogan MP, Dunne JE, Fernández-Moreira V, Hess JB, Hayes AJ, Lloyd D, Millet C, Pope SJ, Williams C (2007) Rhenium fac tricarbonyl bisimine complexes: biologically useful fluorochromes for cell imaging applications. Chem Commun 3066–3068
161. Koike K, Okoshi N, Hori H, Takeuchi K, Ishitani O, Tsubaki H, Clark IP, George MW, Johnson FP, Turner JJ (2002) Mechanism of the photochemical ligand substitution reactions of fac-$[Re (bpy)(CO)_3(PR_3)]^+$ complexes and the properties of their triplet ligand-field excited states. J Am Chem Soc 124:11448–11455
162. Pierri AE, Pallaoro A, Wu G, Ford PC (2012) A luminescent and biocompatible PhotoCORM. J Am Chem Soc 134:18197–18200
163. Antony LAP, Slanina T, Šebej P, Šolomek T, Klán P (2013) Fluorescein analogue xanthene-9-carboxylic acid: a transition-metal-free CO releasing molecule activated by green light. Org Lett 15:4552–4555
164. Peng P, Wang C, Shi Z, Johns VK, Ma L, Oyer J, Copik A, Igarashi R, Liao Y (2013) Visible-light activatable organic CO-releasing molecules (PhotoCORMs) that simultaneously generate fluorophores. Org Biomol Chem 11:6671–6674
165. Kabanov AV, Batrakova EV, Alakhov VY (2002) Pluronic® block copolymers as novel polymer therapeutics for drug and gene delivery. J Control Release 82:189–212
166. Fraix A, Kandoth N, Manet I, Cardile V, Graziano AC, Gref R, Sortino S (2013) An engineered nanoplatform for bimodal anticancer phototherapy with dual-color fluorescence detection of sensitizers. Chem Commun 49:4459–4461